Exosomes-Based Humoral Regulation of Iron Metabolism is Required for Host Antibacterial Response

Huijuan Kuang
State Key Laboratory of Military Stomatology, Center for Tissue Engineering, School of Stomatology, The Fourth Military Medical University

Geng Dou
State Key Laboratory of Military Stomatology, Center for Tissue Engineering, School of Stomatology, The Fourth Military Medical University

Linfeng Cheng
Department of Medical Microbiology and Parasitology, The Fourth Military Medical University

Xiangdong Wang
State Key Laboratory of Military Stomatology, Center for Tissue Engineering, School of Stomatology, The Fourth Military Medical University

Haokun Xu
State Key Laboratory of Military Stomatology, Center for Tissue Engineering, School of Stomatology, The Fourth Military Medical University

Xuemei Liu
State Key Laboratory of Military Stomatology, Center for Tissue Engineering, School of Stomatology, The Fourth Military Medical University

Feng Ding
State Key Laboratory of Military Stomatology, Center for Tissue Engineering, School of Stomatology, The Fourth Military Medical University

Xiaoshan Yang
Stomatology Hospital, Southern Medical University

Siying Liu
State Key Laboratory of Military Stomatology, Center for Tissue Engineering, School of Stomatology, The Fourth Military Medical University

Lili Bao
State Key Laboratory of Military Stomatology, Center for Tissue Engineering, School of Stomatology, The Fourth Military Medical University

Huan Liu
Department of Otolaryngology Head and Neck Surgery, Peking University Third Hospital

Bei Li

School of Stomatology, Fourth Military Medical University

Yan Jin

Fourth Military Medical University https://orcid.org/0000-0002-2586-1152

Shiyu Liu (liushiyu@vip.163.com)

State Key Laboratory of Military Stomatology, Center for Tissue Engineering, School of Stomatology, The Fourth Military Medical University

---

Article

Keywords:

Posted Date: March 14th, 2022

DOI: https://doi.org/10.21203/rs.3.rs-1425408/v1

Exosomes-Based Humoral Regulation of Iron Metabolism is Required for Host Antibacterial Response

Huijuan Kuang[1#], Geng Dou[1#], Linfeng Cheng[2], Xiangdong Wang[1], Haokun Xu[1], Xuemei Liu[1], Feng Ding[1], Xiaoshan Yang[3], Siying Liu[1], Lili Bao[1], Huan Liu[4], Bei Li[1], Yan Jin[1*], Shiyu Liu[1*]

[1] State Key Laboratory of Military Stomatology & National Clinical Research Center for Oral Diseases & Shaanxi International Joint Research Center for Oral Diseases, Center for Tissue Engineering, School of Stomatology, The Fourth Military Medical University, Xi'an, Shaanxi, 710032, China

[2] Department of Medical Microbiology and Parasitology, The Fourth Military Medical University, Xi'an, Shaanxi, 710032, China

[3] Stomatology Hospital, Southern Medical University, Guangzhou, Guangdong, 510280, China

[4] Department of Otolaryngology Head and Neck Surgery, Peking University Third Hospital, Beijing, 100191, China

[#]These authors contributed equally:
Huijuan Kuang, Geng Dou.

*Correspondence to:
Shiyu Liu, Email: liushiyu@vip.163.com
Yan Jin, Email: yanjin@fmmu.edu.cn

Abstract

Immediate iron restriction by the host is a critical process to protect against bacterial infections. Although the cell-dependent iron sequestration mechanism in liver or spleen has been identified, it is still unclear that whether the host launched humoral regulation mechanism to promptly acquire iron that widely distributes throughout body fluids. Here, we showed that after bacterial invasion, host immediately releases nanosized exosomes to capture circulating iron-containing proteins, which is required for prompt systemic iron sequestration and antibacterial defense. Mechanistically, in a sepsis model, we found that *Salmonella Typhimurium* induces endoplasmic reticulum stress in macrophages and activates inositol requiring enzyme 1α (IRE1α) signaling, triggering lysosomal dysfunction and promoting exosome release. These exosomes bearing transferrin receptors, CD163 and CD91 bind multiple iron-containing proteins, prevent bacteria from iron acquisition, and recycle them to tissue-resident macrophages, ultimately sequestering iron and protecting against infection. Our findings reveal a previously unknown humoral regulation mechanism of iron metabolism during bacterial infection, and suggest the release and circulation of extracellular vesicles could be an important way to promptly regulate systemic ion metabolism.

Introduction

Bacterial infection can lead to bacteremia or even sepsis, threatening human life in serious cases[1]. Since iron participates in critical biological processes including nucleic acid synthesis, electron transport and redox reactions[2] in both host and bacterial pathogens, the host immediately restricts the availability of iron after bacterial invasion and thereby limits the infection, which termed nutritional immunity[2]. It has been well proved that liver- and spleen-resident macrophages take up iron-containing proteins via membrane receptors, including transferrin receptor (TfR), LDL-related protein 1 (CD91), and hemoglobin-haptoglobin receptor (CD163), which bind transferrin-bound iron, heme-hemopexin, and hemoglobin-haptoglobin, respectively, to recycle and sequester iron and thus starve bacteria[3, 4]. These studies focus on cell-dependent regulation of iron metabolism. Given that the iron-containing proteins existing in body fluid may be distant from tissue-resident macrophages and can be acquired by the invading bacteria[2], it is reasonable to hypothesize that the host had evolved undiscovered humoral regulation mechanisms to promptly acquire and recycle the circulating iron for rapid iron sequestration.

Exosomes are extracellular vesicles with diameters of 40-150 nm and are released by cells into multiple body fluids[5, 6], while the role of exosomes in infection are largely unknown. Interestingly, emerging evidence indicates that exosome release during infection may be associated with iron metabolism. First, several studies have found that circulating exosomes highly increase in response to bacterial infection[7, 8]. In addition, circulating exosomes are captured mainly by liver or spleen macrophages[9], which is consistent with the route of iron recycling by the host during bacterial infection. Moreover, exosomes can inherit the membrane characteristics of their parent cells[10, 11], which indicates that exosomes released from liver or spleen macrophages may contain membrane receptors to bind iron-containing proteins. Interestingly, regarding the physical properties, the nanosized exosomes show a high diffusion coefficient, and a high surface-to-volume ratio which is related to superior adsorptive capacity. These properties facilitate exosomes to diffuse rapidly and affect distant cells or tissues[12], and to protect host cells by serving as decoys that bind bacterial toxin[13]. Therefore, we hypothesize that exosomes released by the host could bind and preserve iron-

containing proteins, then recycle them back to macrophages, serving as circulating humoral "iron catchers" to prevent bacteria from iron acquisition.

In this study, we found *Salmonella Typhimurium* (*S*.Tm) induces endoplasmic reticulum stress (ERS) of host macrophages and activates inositol requiring enzyme 1α (IRE1α) signaling, triggering lysosomal dysfunctions and promoting exosome release. These exosomes bearing receptors such as transferrin receptor bind iron-containing proteins, prevent bacteria from iron acquisition, and recycle iron to tissue-resident macrophages, ultimately protecting against infection (**Graphical Abstract**). Taken together, these findings reveal a previously unknown humoral regulation mechanism of iron metabolism during bacterial infection, broaden the knowledge of iron metabolism as cellular and humoral manner. The findings also reveal the role of exosomes in nutritional immunity, and suggest the release and circulation of extracellular vesicles could be an important way to promptly regulate systemic ion metabolism.

Graphical Abstract

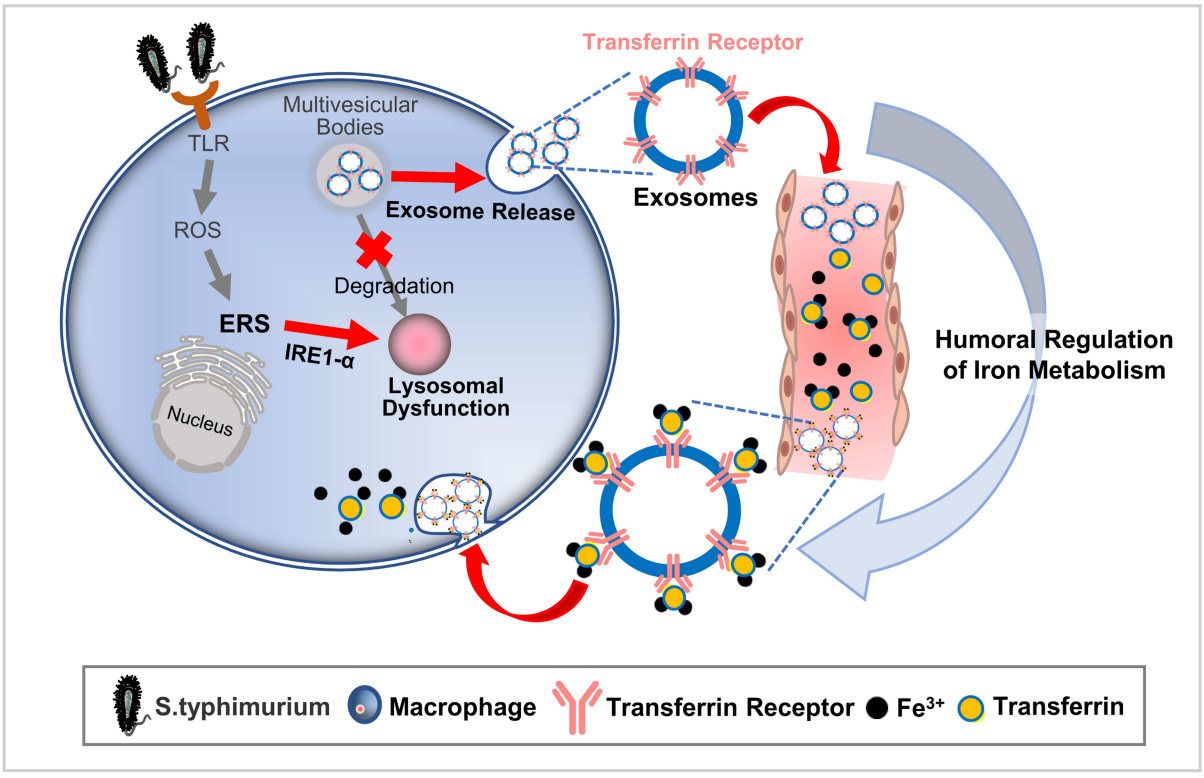

Results

Host exosome release is required for prompt iron sequestration and resistance to bacterial infection

Immediate restriction of iron has been viewed as a critical innate defense mechanism against bacterial infection[14]. We first confirmed the changes in iron distributions in mice infected with *S.*Tm, a gram-negative bacterium, frequently causes microbial sepsis[15]. As expected, the number of *S.*Tm increased quickly in blood after infection (**Extended Data Fig.1a**), and the serum iron level declined markedly, while hepatic and splenic iron levels significantly increased (**Extended Data Fig.1b**), similar to prior studies showing an alteration in iron distributions after *S.*Tm infection[16, 17]. Importantly, we found that the exosome concentration in serum was upregulated at 3 hours after infection and continued to increase within 24 hours (**Extended Data Fig.1c**), suggesting that immediately elevating exosome level is a feature of host response to infection. To explore the biodistribution of serum exosomes, the DiR-labeled exosomes were intravenously injected into mice. *Ex vivo* fluorescent imaging revealed that most of the infused exosomes homed to the liver or spleen (**Extended Data Fig.2a**). Furthermore, confocal images showed that the infused exosomes were mainly taken up by liver or spleen $F4/80^+$ macrophages (**Extended Data Fig.2b and 2c**). These data suggest that the biodistribution of circulating exosomes is consistent with that of systemic iron after bacterial infection. However, the role of infection-induced host exosome release in iron metabolism and infection outcomes is still unknown.

To answer this question, we used GW4869, which has been successfully utilized to inhibit exosome release *in vitro* and *in vivo*[18, 19], to block host exosome release during infection (**Fig.1a**). The results showed that, *S.*Tm-induced elevation of circulating exosomes was significantly inhibited in mice subjected to GW4869 pretreatment (**Fig.1b**). Moreover, compared to *S.*Tm-infected mice, serum iron level significantly increased in *S.*Tm-infected mice pretreated with GW4869 (**Fig.1c**). These findings demonstrate that blockade of exosome release disrupts iron sequestration in mice during infection.

Next, we investigated the effects of exosome release blockade on the host defense response to infection. We found that, compared to *S.*Tm-infected mice, the viable count of *S.*Tm increased markedly in blood of *S.*Tm-infected mice pretreated with GW4869 (**Fig.1d**). Histologic examination of the liver showed inflammatory infiltration at 12 hours after bacterial infection. Severe liver injury was found at 4 days after *S.*Tm infection compared to uninfected control mice, shown by gross lesions accompanied by inflammatory infiltration and elevated histological scores (**Fig.1e**). More importantly, the infected mice pretreated with GW4869 showed large areas of extensive cellular necrosis with loss of hepatic architecture and more severe inflammatory cell infiltration (**Fig.1e**). Liver injury was also examined by measuring the levels of aspartate aminotransferase (AST) and alanine aminotransferase (ALT) in serum. Compared with uninfected control mice, *S.*Tm-infected mice showed elevated levels of ALT and AST in the sera. Pretreatment with GW4869 significantly enhanced serum ALT and AST levels in the infected mice (**Fig.1f**). Next, morphological changes in the spleen were investigated. At 12 hours after infection, no obvious histological alterations were observed in the spleen (**Fig.1g**). At 4 days after infection, the spleens from the infected mice displayed a distinctly irregular histology, and a significant loss of the distinct borders between the red and white pulp regions. Moreover, the infected mice pretreated with GW4869 exhibited more severe spleen injuries and elevated histological scores (**Fig.1g**). Splenomegaly is common following bacterial infection. Accordingly, we found *S.*Tm infection increased the spleen weight with significant increase in spleen weights observed in the GW4869-pretreated group (**Fig.1h**). As long-term mortality is associated with sustained injury, survival experiments were performed[20]. Compared with PBS treated control mice, *S.*Tm-infected mice or *S.*Tm-infected mice pretreated with GW4869 showed 100% mortality, while GW4869 pretreatment greatly shortened the mouse survival time (**Fig.1i**). These results suggest that blockade of host exosome release disturbs iron sequestration, increases iron availability, and worsens the outcomes of infection.

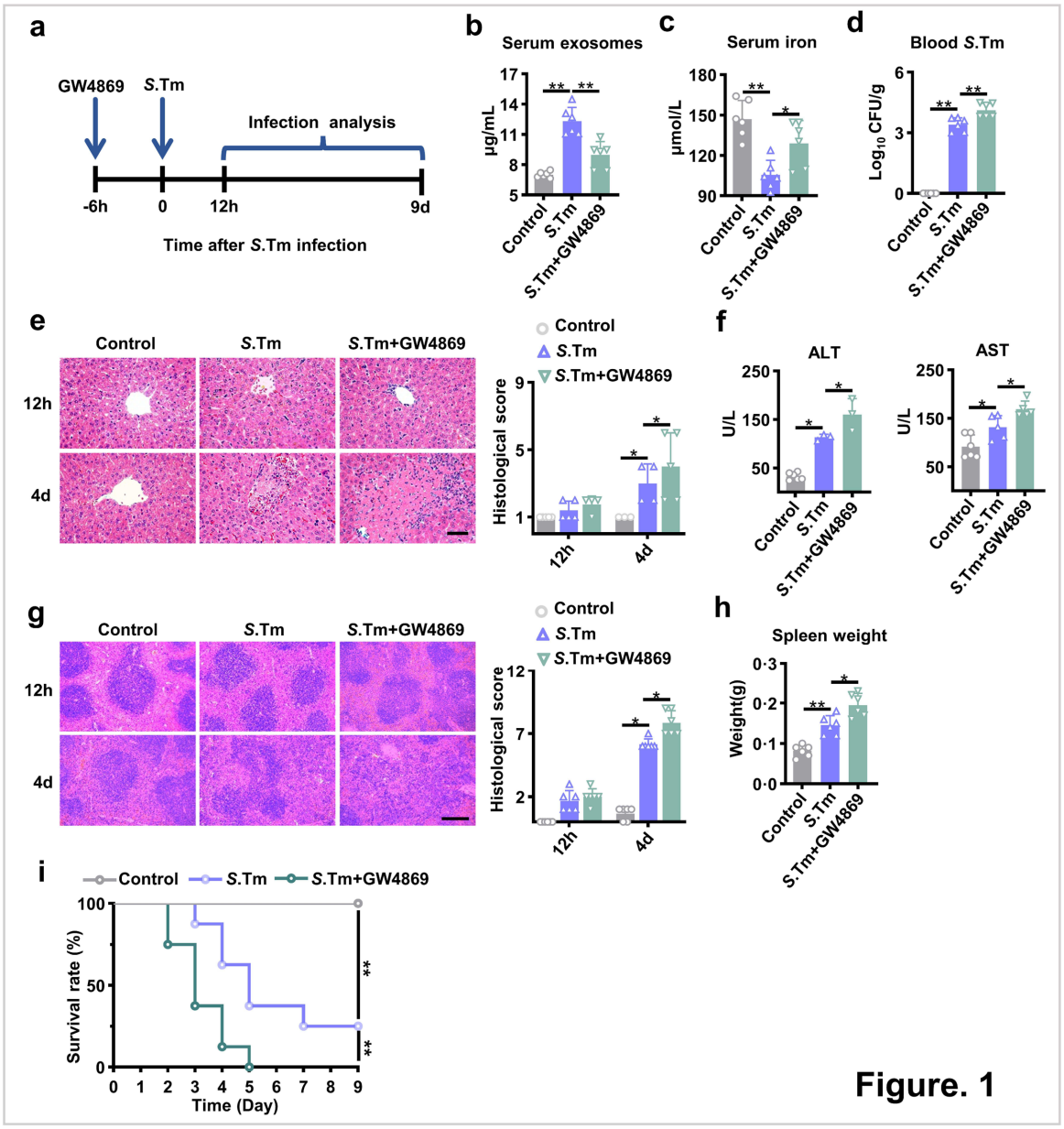

Fig. 1 Blockade of host exosome release increases the susceptibility of mice infected with *S*.Tm.

a, Schematic diagram of the experimental procedure. To evaluate the effects of exosome release blockade on the host defense response to infection, *S*.Tm-infected mice were pretreated with GW4869 to block exosome release. **(b-d),** The control mice, *S*.Tm-infected mice, and *S*.Tm-infected mice pretreated with GW4869 were euthanized at 12 hours after *S*.Tm infection for further analysis. **b,** The concentration of exosomes in serum. n = 6 mice. **c,** The iron level in serum. n = 6 mice. **d,** Viable count of *S*.Tm in the blood. n=6 mice. **e,** H&E staining of representative liver sections and the associated histological scores at 12 hours or day 4 after infection. Scale bar, 50 μm. n = 6 mice. **f,** ALT and AST levels in the serum at day 4 after infection. n = 6 mice in the control group. n = 3-5 mice in other groups. **g,** H&E staining of representative tissue sections of spleen at 12 hours or day 4 after infection, and the associated histological scores. Scale bar, 250 μm. n = 6 mice. **h,** The spleen weights at day 4 after infection. n = 6 mice. **i,** Survival rates of mice. n = 6 mice. For **b-h**, data are presented as the mean ± s.d. For **b-f**, and **h**, statistical significance was assessed by one-way ANOVA with Tukey's post-hoc test. For **g**, statistical significance was assessed by the Kruskal-Wallis test. For **i**, statistical significance was performed using the log-rank test. *p < 0.05, **p < 0.01, ns, not significant.

We further investigated the role of host exosomes in iron metabolism and infection defense. We first isolated exosomes from the serum of uninfected or *S.*Tm-infected mice by ultracentrifugation. The isolated exosomes were both positive for the exosome markers CD63, CD81, TSG101 and Alix but lacked the mitochondrial marker calnexin (**Fig.2a**). NTA showed that more than 90% of the exosomes were within the 30-120 nm range, and the mean size of exosomes derived from the serum of uninfected mice or *S.*Tm-infected mice were 110 nm and 116 nm, respectively (**Fig.2b**). A typical circular or elliptical morphology was also visible in TEM images (**Fig.2c**). These data show that *S.*Tm infection does not substantially affect the marker expression, size or shape of exosomes in serum. Next, to investigate the functions of exosomes, GW4869-pretreated infected mice were intravenously injected with exosomes derived from uninfected or *S.*Tm-infected mouse serum (**Fig.2d**). Administration of exosomes caused markedly decreased levels of iron in serum, especially in mice treated with exosomes derived from infected mouse serum (**Fig.2e**). We also found that exosome treatment resulted in decreased number of bacteria in the blood, which was more evident in mice treated with exosomes derived from infected mouse serum (**Fig.2f**). Regarding the histological analysis, at 4 days but not 24 hours post-infection, the *S.*Tm-infected mice pretreated with GW4869 developed substantial liver (**Fig.2g**) and spleen injury (**Fig.2h**). However, exosome administration could ameliorate liver and spleen injury. In particular, compared to exosomes from uninfected mouse serum, exosomes from *S.*Tm-infected mouse serum more effectively improved hepatopathological changes such as attenuated liver injury area and inflammatory infiltration **(Fig.2g),** alleviated pathological lesions and improved splenic structure in the spleen (**Fig.2h**). Meanwhile, treatment with exosomes derived from infected mouse serum significantly reduced liver (**Fig.2g**) and spleen injury scores (**Fig.2h**) and alleviated spleen enlargement (**Fig.2i**). Importantly, exosome treatment also improved survival under sepsis. While most of the GW4869-pretreated septic mice died within 5 days, GW4869-pretreated septic mice treated with serum exosomes had a higher survival rate, especially in the mice treated with exosomes derived from *S.*Tm-infected mouse serum (**Fig.2j**). These data demonstrate that bacterial infection induces immediate release of exosomes, facilitating prompt iron sequestration and protecting against bacterial infection.

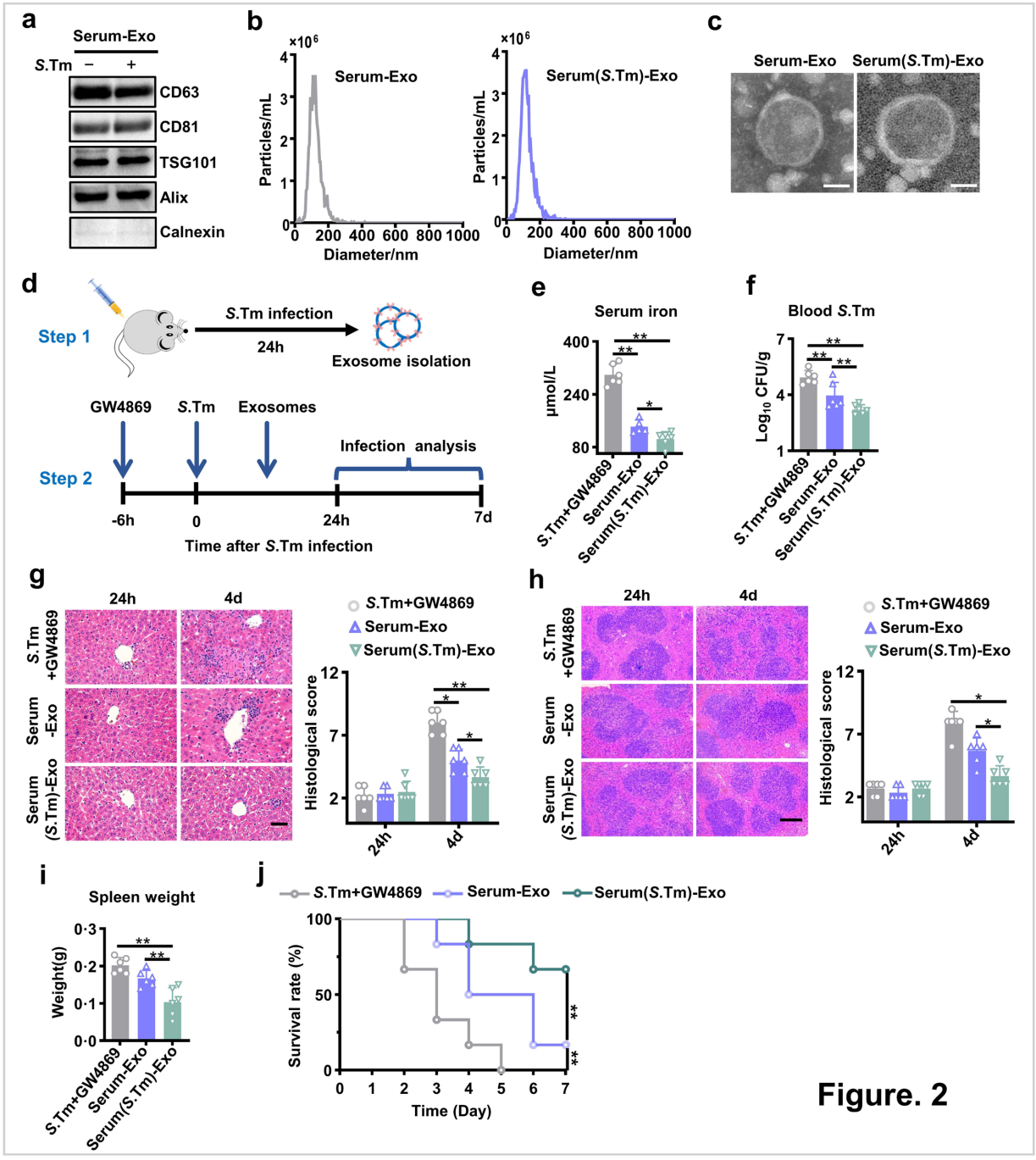

Fig. 2 Supplementation with serum exosomes decreases the infection severity by *S*.Tm in exosome release-deficient mice.

(a-c), The mice were intraperitoneally injected with *S*.Tm for 24 hours and the serum was collected. Exosomes were isolated from the uninfected mouse serum (Serum-Exo group) or *S*.Tm-infected mouse serum [Serum(*S*.Tm)-Exo group] and characterized. **a,** Western blot analysis of the exosome markers Alix, CD81, CD63 and TSG101, and the negative mitochondrial marker calnexin. **b,** NTA analysis of the concentration and size distribution of exosomes. **c,** TEM analysis of exosomes. Scale bar, 50 nm. **d,** Schematic diagram of the *in vivo* experimental procedure. Exosomes were isolated from uninfected mouse serum or *S*.Tm-infected mouse serum (Step 1). To investigate the role of host exosomes in iron metabolism and infection outcomes, GW4869-pretreated *S*.Tm-infected mice were injected with exosomes derived from uninfected mouse serum (Serum-Exo group) or exosomes derived from *S*.Tm-infected mouse serum [Serum(*S*.Tm)-Exo group], and the mice were euthanized

for further analysis (Step 2). **e,** The iron level in serum. n = 6 mice. **f,** Viable count of *S*.Tm in blood. n = 6 mice. **g, h,** Representative H&E staining of the liver **(g)** and spleen **(h)** at 24 hours or day 4 after *S*.Tm infection and quantitative analysis of histological scores. Scale bar, 50 μm **(g)** and 250 μm **(h)**. n = 6 mice. **i,** The spleen weight at day 4 after infection. n = 6 mice. **j,** Survival rate of mice. n=6 mice. For **e-i**, data are presented as the mean ± s.d. For **e**, statistical significance was assessed by the Kruskal-Wallis test. For **f-i**, statistical significance was assessed by one-way ANOVA with Tukey's post-hoc test. For **j**, statistical significance was performed using the log-rank test. *$p < 0.05$, **$p < 0.01$, ns, not significant.

We next investigated which kind of cells could release exosomes that have iron metabolism regulation functions. It has been proven that macrophages have a precise regulatory system to maintain iron homeostasis during bacterial infection[21]. Therefore, we utilized primary bone marrow-derived macrophages (BMDM), a model widely used as prototypical macrophages for *in vitro* studies[22], to investigate exosome functions. We isolated and characterized exosomes from supernatants of BMDM treated with *S*.Tm or PBS. Analysis of marker expression **(Extended Data Fig.3a)**, particle size (**Extended Data Fig.3b**), and morphology (**Extended Data Fig.3c**) showed that the isolated BMDM-exosome fractions were pure and that *S*.Tm infection did not alter the general properties of the exosomes. Next, these exosomes were systemically injected into infected mice pretreated with GW4869 (**Extended Data Fig.3d**). The serum iron levels declined markedly only in infected mice injected with exosomes derived from *S*.Tm-treated BMDM (**Extended Data Fig.3e**). Concomitantly, the number of *S*.Tm decreased markedly in blood (**Extended Data Fig.3f**). The administration of exosomes derived from infected BMDM reduced the liver (**Extended Data Fig.3g**) and spleen injury (**Extended Data Fig.3h, i**). Ultimately, the injection of exosomes from infected BMDM extended the survival of septic mice pretreated with GW4869 (**Extended Data Fig.3j**). These results demonstrate that exosomes released by macrophages are involved in iron sequestration, and protect against infection.

Host exosomes bearing multiple iron-related receptors bind iron

We next determined how host exosomes facilitate iron sequestration. During bacterial infection, macrophages take up iron or iron-containing molecules via receptors, including TfR, CD91, and CD163[23]. Given that we found exosomes released by *S*.Tm-infected BMDM participating in iron

sequestration, we wondered whether exosomes released by macrophages expressed these iron-related receptors and directly bound iron or iron-containing molecules. We hypothesized that exosome-based iron sequestration could serve as an efficient strategy for promptly iron recycling during infection. We therefore isolated exosomes form mouse serum and BMDM culture supernatants, and detected iron-related receptor expression. We found that exosomes derived from serum (**Fig.3a, left**) or BMDM (**Fig.3a, right**) expressed TfR, CD91, and CD163, which were significantly upregulated under *S*.Tm infection conditions. Further determination of TfR, CD91, and CD163 localization was performed by immunoelectron microscopy[24], and the results showed that TfR, CD91, and CD163 were present on the surface of serum exosomes (**Fig.3b**) or BMDM-derived exosomes (**Fig. 3c**).

Next, we determined whether these exosomes bind iron or iron-containing molecules to sequester iron in serum for inhibiting bacterial growth. Exosomes derived from infected or uninfected mouse serum were added to the exosome-depleted mouse serum. After incubation, the added exosomes were isolated by ultracentrifugation, and serum supernatant was collected for iron amount analysis or for *S*.Tm culture (**Fig.3d**). The results showed that the addition of exosomes derived from *S*.Tm-infected mouse serum but not uninfected mouse serum induced significant decrease in iron levels (**Fig.3e**), which may be because exosomes derived from the infected mouse serum expressed higher levels of iron-related receptors (**Fig.3a, left**) and could bind iron-containing molecules. In the host, Fe exists in multiple forms including transferrin, ferritin, hemoglobin, and other iron-containing proteins[25]. Transferrin is the major iron shutter in the circulation[26] and is a critical source of iron for bacteria during infection[27]. Given that TfR expression in exosomes from infected mice was significantly upregulated (**Fig.3a, left**), we next determined the ability of exosomes to bind transferrin. After exosome incubation, the transferrin concentration was decreased in the serum supernatant (**Fig.3f**). The incubation of exosomes derived from infected mouse serum caused a greater decrease in transferrin concentration (**Fig.3f**). In addition, to further prove the binding ability of exosomes, the added exosomes were isolated, and the transferrin level in the exosomal fraction was measured. The results showed that the transferrin level in exosomes derived from

infected mouse serum was significantly higher than that in exosomes derived from uninfected mouse serum (**Fig.3g**). These results demonstrate that exosomes sever as "iron catchers" via membrane-bearing receptors such as TfR. To further determine whether exosomes could protect the captured iron from bacterial acquisition, exosomes derived from infected mouse serum were incubated with *S*.Tm. The fluorescence images showed rare uptake of exosomes by *S*.Tm (**Fig.3h**), which indicated that *S*.Tm could not directly acquire iron by exosome uptake. Therefore, these data demonstrate that exosomes can prevent bacteria from iron acquisition.

The *S*.Tm is a highly iron-dependent bacterial pathogen[28]. As exosomes derived from infected mouse serum induced the significant decrease in iron and transferrin levels in serum supernatant (**Fig.3e, f**), we then determined whether this serum supernatant is unfavorable for bacterial growth after exosomes binding iron. Serum supernatant after incubation with exosomes derived from infected mouse serum was inoculated with *S*.Tm (**Fig.3d**), and significant differences in their growth curves were observed, including in the overall pattern of the growth curve, lag phase and peak doubling time (**Fig.3i**). We found that, compared with control serum, *S*.Tm grew more slowly in the serum supernatant which was incubated with exosomes derived from infected mouse serum (**Fig.3i**), while supplementation with iron-dextran in this serum supernatant partially recovered *S*.Tm growth (**Fig.3i**). We then performed the same experiment to detect whether the exosomes derived from infected BMDM had the ability to bind iron or iron-containing molecules. Meanwhile, to prove certain receptor-mediated iron binding, before *S*.Tm infection, BMDM were transfected with TfR siRNA to knockdown the expression in exosomes (**Extended Data Fig.4**). The results showed that exosomes derived from infected BMDM induced greater decreases in total iron (**Fig.3j**) and transferrin levels (**Fig.3k**) than exosomes derived from uninfected BMDM or infected BMDM with TfR knockdown. After incubation in serum, the transferrin level in isolated exosomes derived from infected BMDM was also significantly higher than that of exosomes derived from uninfected BMDM or infected BMDM with TfR knockdown (**Fig.3l**). Similarly, *S*.Tm grew more slowly in the serum supernatant which was incubated with exosomes derived from infected BMDM (**Fig.3m**). These results suggest that exosomes released during infection inhibit *S*.Tm growth by binding iron.

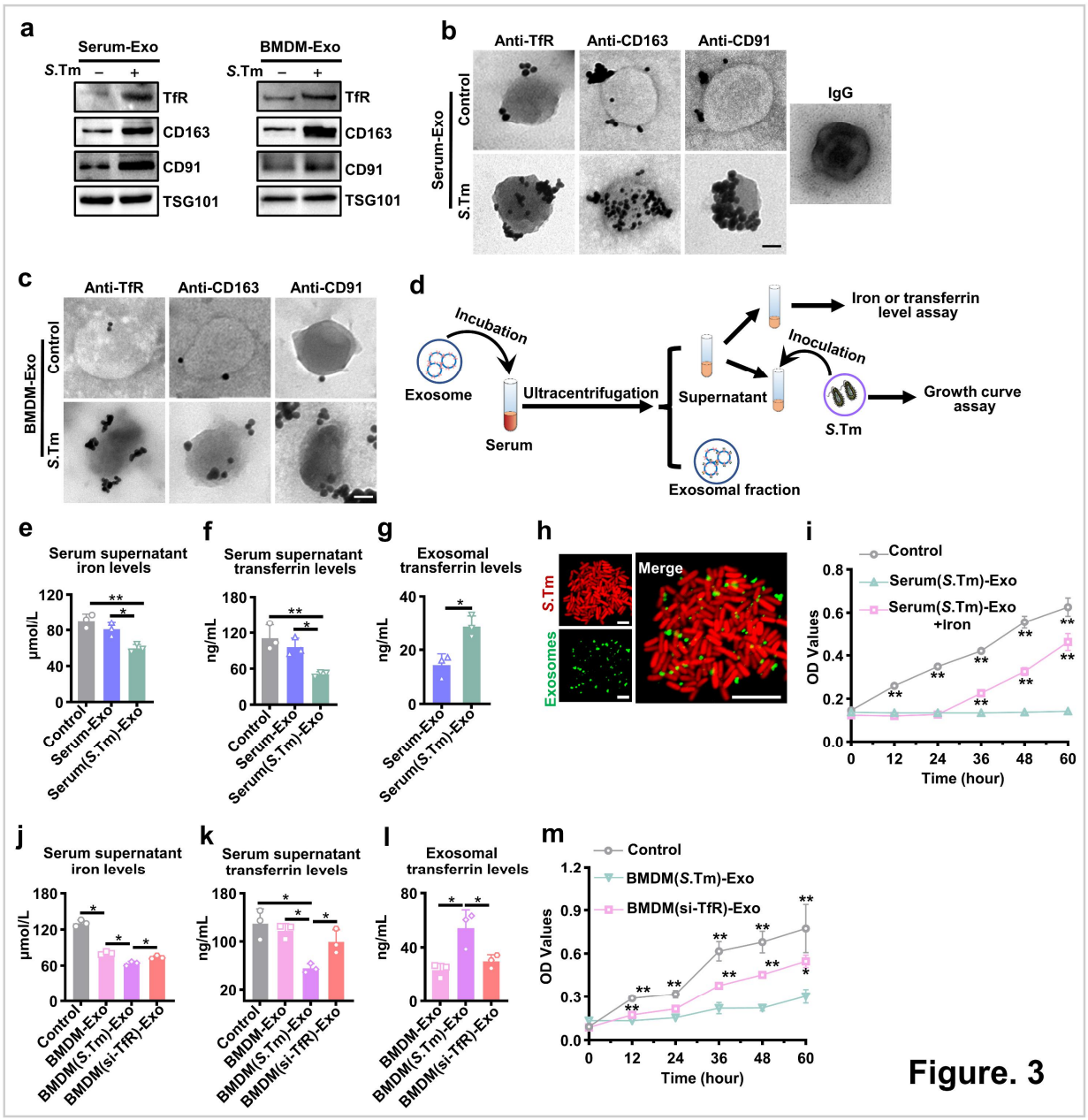

Fig. 3 TfR-, CD163-, and CD91-bearing exosomes derived from *S*.Tm-infected serum or BMDM bind iron. **(a-c),** Normal mice were intraperitoneally injected with *S*.Tm for 24 hours and serum exosomes were isolated. BMDM were infected with *S*.Tm for 24 hours *in vitro* and supernatant exosomes were isolated. **a,** Western blot analysis of TfR, CD163, CD91 and TSG101 expression in exosomes derived from uninfected or infected mouse serum (left), and in exosomes released from uninfected or infected BMDM (right). **b,** Immunoelectron microscopy detection of TfR, CD163, CD91 and isotype control IgG antibodies in exosomes derived from uninfected or infected mouse serum. Scale bar, 50 nm. **c,** Immunoelectron microscopy detection of TfR, CD163, and CD91 in exosomes derived from uninfected or infected BMDM. Scale bar, 50 nm. **d,** Schematic diagram of the experimental design to test the ability of exosomes to bind iron in serum. Serum was incubated with exosomes derived from uninfected mouse serum (Serum-Exo group) or infected mouse serum [Serum(*S*.Tm)-Exo group] for 12 hours. Then the exosomes were isolated by ultracentrifugation. The exosomal fraction and serum supernatant were used for further analysis. **e, f,** Total iron levels **(e)** and transferrin levels **(f)** in the serum supernatant. n = 3 biologically independent samples. **g**, Transferrin levels in exosomal fractions derived from

uninfected or infected mouse serum. n = 3 biologically independent samples. **h**, Representative fluorescence images of *S*.Tm expressing mCherry (red) incubated with exosomes (green) derived from infected mouse serum. Scale bars, 10 μm. n = 3 biologically independent samples. **i**, Growth curve of *S*.Tm in serum supernatant. n = 5 biologically independent samples. **j-m**, Serum was incubated with exosomes released from BMDM (BMDM-Exo group), BMDM infected with *S*.Tm [BMDM(*S*.Tm)-Exo group] or infected BMDM transfected with TfR siRNA [BMDM(si-TfR)-Exo group]. Then the exosomes were isolated and serum supernatant was collected for analysis. **j, k,** Total iron levels **(j)** and transferrin levels **(k)** in the serum supernatant. n = 3 biologically independent samples. **l**, Transferrin levels in exosomal fraction. n = 3 biologically independent samples. **m**, Growth curve of *S*.Tm in serum supernatant. n = 5 biologically independent samples. For **e-g** and **i-m**, data are presented as the mean ± s.d. For **e, f, j-l**, statistical significance was assessed by one-way ANOVA with Tukey's post hoc test. For **g**, statistical significance was assessed by unpaired two-tailed Student's t test. For **i** and **m**, statistical significance was assessed by one-way ANOVA with Tukey's post-hoc test and Kruskal-Wallis test. *p < 0.05, **p < 0.01, ns, not significant.

We proved that the iron-related receptors, including TfR, CD91, and CD163, were upregulated in exosomes released from *S*.Tm-infected mice or BMDM, so we wondered whether this represents a general mechanism used by host cells to bind iron and limit iron access by bacteria. We next used gram-positive *Staphylococcus aureus* (*S*.a), which is an important cause of sepsis[29], to infect mice and BMDM. Consistent with our findings, the expression levels of TfR, CD91, and CD163 in exosomes derived from serum (**Extended Data Fig.5a left**) or BMDM (**Extended Data Fig.5a right**) were all elevated after *S*.a infection. The immunoelectron microscopy images further confirmed the surface location of these receptors (**Extended Data Fig.5b**)**.** We also detected the iron binding capacity of these exosomes in serum (**Extended Data Fig.5c**). Incubation with exosomes derived from *S*.a-infected mouse serum induced significant decrease in total iron (**Extended Data Fig.5d**) and transferrin levels (**Extended Data Fig.5e**) in serum supernatant. When the serum supernatant with lower iron levels was inoculated with *S*.a, the growth rates were significantly decreased (**Extended Data Fig.5f**). Therefore, we found that during bacterial infection, the levels of iron-related receptors including TfR, CD91, and CD163 in host exosomes are elevated for prompt iron sequestration, demonstrating a humoral regulation mechanism of iron metabolism.

Host exosome-induced prompt hypoferremia protects against bacterial infection

Although we found that exosome release is required for prompt iron sequestration and resistance to infection and that exosomes can bind iron-containing molecules, the protective effects generated by host exosomes during infection still require further clarification. During infection, serum iron content is downregulated in a timely manner by the host to induce hypoferremia[30], which has been considered a critical defense mechanism to restrict iron availability to invading pathogens[31, 32]. We then determined whether the iron-binding capability of exosomes was involved in the development of rapid hypoferremia. To evaluate the protective effects of exosomes induced by *S*.Tm infection, we used heat-killed *S*.Tm (HK*S*.Tm) to induce host exosomes release while avoiding lethal virulence (**Fig.4a**). The HK*S*.Tm has been proven to be recognized by the same mechanism as *salmonella*[33]. As expected, compared with *S*.Tm-infected mice, pretreatment of HK*S*.Tm before *S*.Tm infection led a significant increase in exosomes in serum (**Fig.4b**). Moreover, infected mice pretreated with HK*S*.Tm led to a marked drop in serum iron (**Fig.4c**) and a decreased number of *S*.Tm in blood (**Fig.4d**). Compared with the liver and spleen injury induced by *S*.Tm infection, pretreatment with HK*S*.Tm attenuated liver (**Fig.4e**) and spleen injury (**Fig.4f**), accompanied by a reduction in injury scores. Pretreatment with HK*S*.Tm also significantly reduced *S*.Tm-induced splenomegaly (**Fig.4g**). In addition, most importantly, compared with *S*.Tm-infected mice, infected mice received HK*S*.Tm pretreatment lived significantly longer (**Fig.4h**). To further clarify the association between the protective effect and exosome release, we used GW4869 to inhibit exosome release (**Fig.4b**). GW4869 treatment significantly attenuated the downregulation of serum iron levels by HK*S*.Tm pretreatment (**Fig.4c**), which subsequently resulted in an increase in *S*.Tm number in blood (**Fig.4d).** Blockade of exosome release by GW4869 also strongly attenuated HK*S*.Tm-mediated protection in infected mice, including liver (**Fig.4e**) and spleen (**Fig.4f, g**) injury. Notably, compared with infected mice pretreated with HK*S*.Tm, GW4869 treatment significantly shortened the survival (**Fig.4h**). The above results demonstrate that during infection, elevated exosome levels cause prompt hypoferremia, which contributes to host defense against infection.

To determine whether the protective effects generated by exosomes was due to iron restriction of bacterial growth, we utilized iron-dextran to increase serum iron levels in infected mice pretreated with HK*S*.Tm (**Fig.4i).** Compared to infected mice pretreated with HK*S*.Tm, iron-dextran treatment

contributed to bacterial replication and high numbers of *S*.Tm in the blood (**Fig.4j**). This resulted in more extensive necrosis in liver (**Fig.4k**) and disturbed architecture in the spleen (**Fig.4l**), elevated histological injury score of liver (**Fig.4k**) and spleen (**Fig.4l**), aggravated splenomegaly (**Fig.4m**), and shortened survival (**Fig.4n**). Taken together, these results demonstrate that host exosomes are released into circulation to trigger prompt iron sequestration and hypoferremia, and consequently restrict iron accessibility and protect against infection.

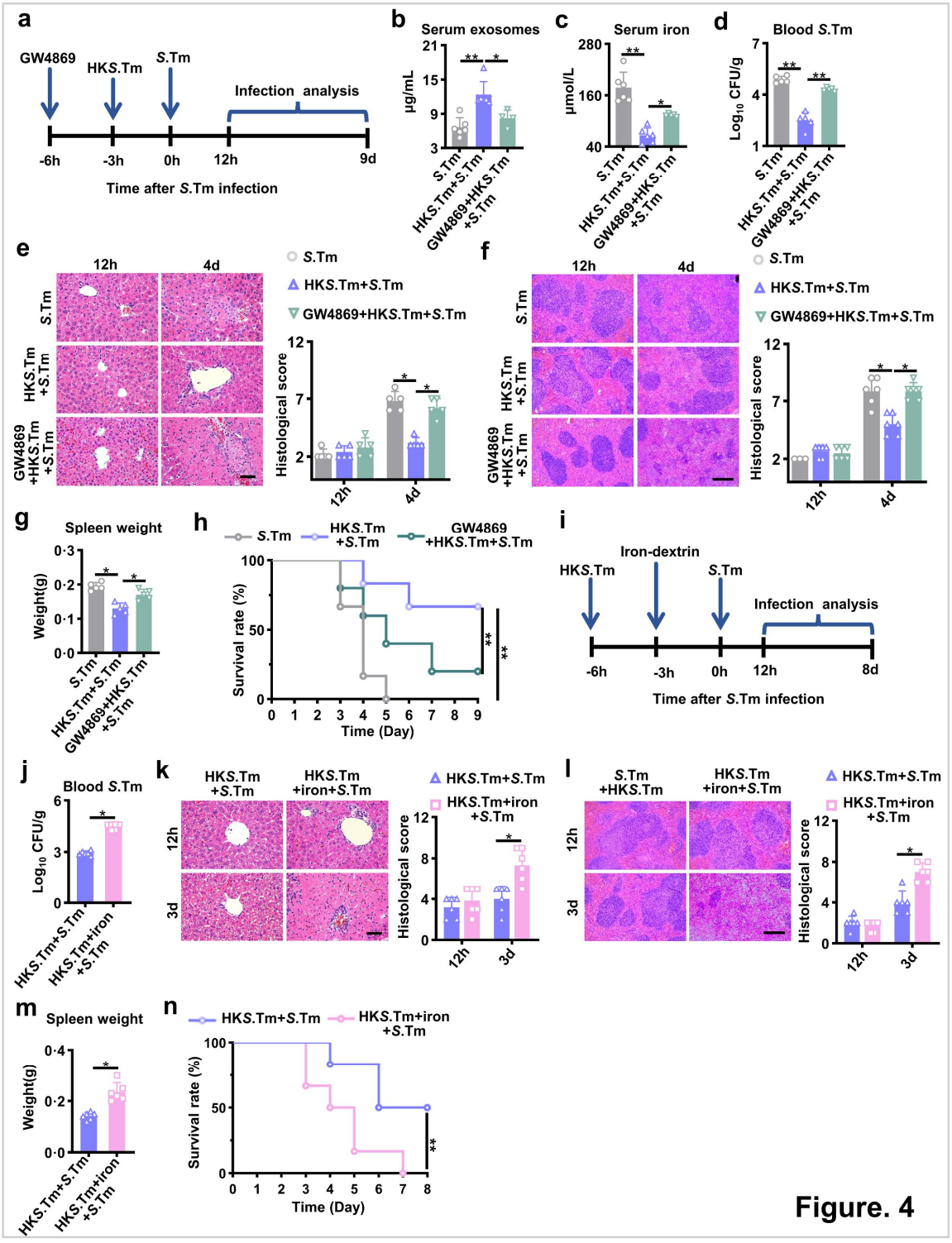

374

Fig. 4 Host exosome-induced hypoferremia protects against bacterial infection.

a, Schematic diagram of the experimental procedure. To evaluate the protective effects of exosomes induced by *S*.Tm infection. HK*S*.Tm was used to induce endogenous exosome release (HK*S*.Tm+*S*.Tm group). Meanwhile, to elucidate the association between exosome release and the protective effect, GW4869 was used to inhibit endogenous exosome release (GW4869+HK*S*.Tm+*S*.Tm group). **b**, The concentration of exosomes in serum. n = 6 mice. **c,** The iron level in serum. n = 6 mice. **d**, Viable count of *S*.Tm in blood at 12 h after *S*.Tm injection. n = 6 mice. **e, f**, Representative H&E staining of the liver **(e)** or spleen **(f)** at 12 hours or day 4 after *S*.Tm infection and histological scores. scale bar, 50 μm **(e)** and 250 μm **(f)**. n = 6 mice. **g**, The spleen weight at day 4 after *S*.Tm infection. n = 6 mice. **h,** Survival rates of mice. n = 6 mice. **(i-n), i,** Schematic diagram of the experimental procedure. To evaluated whether the protective effects generated by exosomes were due to iron restriction of bacterial growth**,** HK*S*.Tm was pretreated to induce endogenous exosome release (HK*S*.Tm+*S*.Tm group). Then, the mice were injected with iron-dextran to increase iron levels before *S*.Tm infection (HK*S*.Tm+iron+*S*.Tm group). **j**, Viable count of *S*.Tm in blood at 12 hours after *S*.Tm injection. n = 6 mice. **k, l,** Representative HE staining of the liver **(k)** and spleen **(l)** at 12 hours and day 3 after *S*.Tm infection and histological scores. Scale bar, 50 μm **(k)** and 250 μm **(l)**. n = 6 mice**. m,** The spleen weights at day 3 after infection. n = 6 mice. **n**, Survival rates of mice. n = 6 mice. For **b-g**, and **j-m**, data are represented as the mean ± s.d. For **c, d, f, and g**, statistical significance was assessed by one-way ANOVA with Tukey's post hoc test. For **b and e**, statistical significance was assessed by the Kruskal-Wallis test. For **j-m**, statistical significance was assessed by unpaired two-tailed Student's t test. For **h** and **n**, statistical significance was assessed by the log-rank test. *$p < 0.05$, **$p < 0.01$, ns, not significant.

Endoplasmic reticulum stress-induced lysosomal dysfunction caused by bacteria infection increases exosome release

Given we have found the important role of host exosome release during infection, we next determined how bacterial invasion induces exosome release. Exosomes are generated by fusion of multivesicular bodies (MVBs) with the plasma membrane[34]. In addition to exocytosis, MVBs can also fuse with lysosome to generate the phagolysosome for degradation[34]. Strong evidence shows that lysosomal dysfunctions caused by various conditions result in increased exocytosis and exosome release[34]. Here, we found significantly reduced lysosome acidity by LysoTracker (fluorescent acidic organelle tracer) in macrophages after *S*.Tm infection *in vitro* (**Fig.5a**), which may account for the enhanced exosome release. More evidence provided by Western blot showed the reduced expressions of ATP6V1A and ATP6V1B, subunits of V-ATPase, in macrophages after *S*.Tm infection (**Fig.5b**), which confirmed the lysosomal dysfunction caused by *S*.Tm infection. To further clarify the relationship of lysosome function and exosome release, we used the V-ATPase

inhibitor bafilomycin A to induce lysosomal dysfunction. As expected, bafilomycin A markedly inhibited the lysosomal acidity (**Fig.5a**) and promoted exosome release (**Fig.5c**), generating similar effects as *S*.Tm infection. Hence, it's plausible that the lysosomal dysfunction caused by infection promotes exosome release (**Fig.5a-c**).

We then investigated how bacterial invasion induces lysosomal dysfunction and exosome release. Lysosomal function has been shown to be closely associated with endoplasmic reticulum stress (ERS)[34], which is activated when cells are subjected to bacterial infection[35]. However, whether ERS caused by bacterial infection controls exosome release by regulating lysosome function has not yet been elucidated. Therefore, we first explored whether ERS was triggered and could regulate lysosomal function in infected macrophages. We found tremendous intracellular reactive oxygen species (ROS) caused by *S*.Tm stimulation (**Fig.5d**). In addition, TEM images showed *S*.Tm infection-induced morphological dilatation of endoplasmic reticulum (**Fig.5e**). At the same time, the expression of ERS-related proteins, including IRE1α, ATF4, ATF6 and GRP78, were evidently upregulated after infection (**Fig.5f**), which is also evidenced by fluorescence images (**Fig.5g**). The elevated intracellular calcium concentration indicated by fluorescence detection also confirmed the ERS in infected macrophages (**Fig.5h, i**). To clarify the association between ERS and lysosomal function, we used the ERS inhibitor 4-phenylbutyric acid (4-PBA)[36] to inhibit ERS response after infection. The TEM images showed 4-PBA treatment significantly inhibited dilatation of endoplasmic reticulum in *S*.Tm-treated macrophages (**Fig.5e**). Additionally, 4-PBA treatment effectively attenuated the upregulated expressions of IRE1α, ATF4, ATF6 and GRP78 (**Fig.5f, g**) and elevated Ca^{2+} levels (**Fig.5h, i**) caused by bacteria infection, which substantiated the ERS inhibition effects of 4-PBA. More importantly, 4-PBA treatment rejuvenate lysosomal acidity in *S*.Tm-treated macrophages, as evidenced by the fluorescence images (**Fig.5j**) and fluorescence OD value (**Fig.5k**). In addition to lysosomal functions, LAMP1 staining showed the lysosome number was obviously reduced in *S*.Tm-treated macrophages, which was also reversed by 4-PBA (**Fig.5l**). Moreover, the decreased expression of ATP6V1A, ATP6V1B and LAMP1 was recovered after 4-PBA treatment (**Fig.5m**). We also found that the level of TFEB, an important transcription factor

that controls lysosomal biogenesis and function[37], was reduced after infection but was partially reversed after 4-PBA treatment (**Fig.5m**). Finally, the ERS inhibition attenuated the elevated exosome release in macrophage induced by *S*.Tm infection (**Fig.5n**). These results demonstrate that ERS triggered by *S*.Tm infection induced lysosomal dysfunction, thereby increasing exosome release.

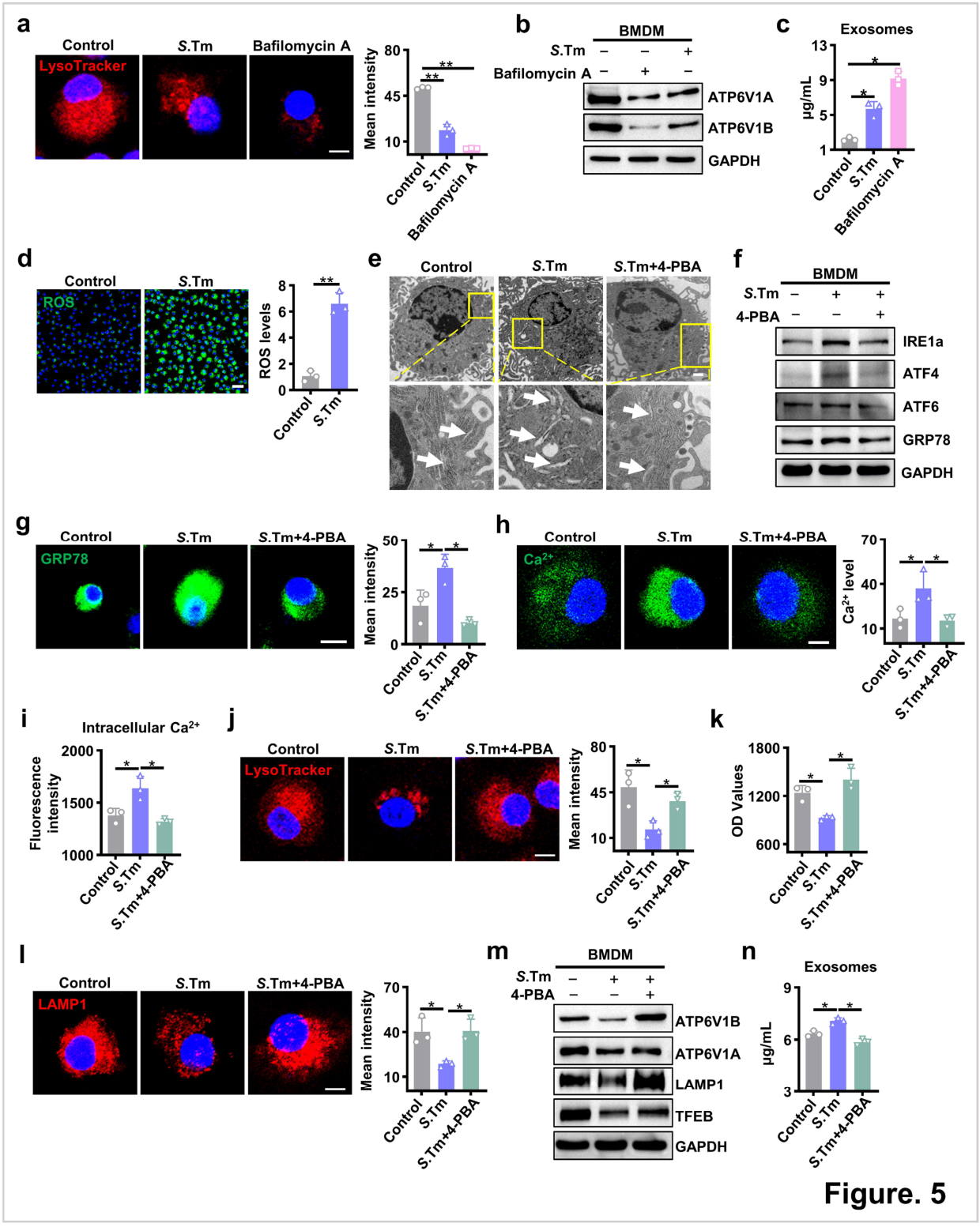

Fig. 5 *S*.Tm infection induces host exosome release via ERS-mediated lysosomal dysfunctions.
(a-c), BMDM were treated with Bafilomycin A or *S*.Tm (MOI: 10) for 24 hours to detect lysosome function and exosome release. **a,** Representative images of LysoTracker staining were detected by laser scanning confocal microscopy and the quantitative fluorescence intensity. Scale bar, 5 μm. **b**, Western blot analysis of the expression of ATP6V1A and ATP6V1B in BMDM. n = 3 biologically independent samples. **c**, The concentration of exosomes released by BMDM. **d**, Representative fluorescence images of ROS in BMDM infected with *S*.Tm for 24 hours, and quantitative analysis of the ROS levels. Scale bar, 50 μm. n = 3 biologically independent samples. **(e-n)**, BMDM were treated with *S*.Tm in the absence or presence of 4-PBA for 24 hours to clarify the association between ERS and exosome release. **e**, The ultrastructural morphology of the endoplasmic reticulum was investigated via TEM. Scale bar, 1 μm. High-magnification images of the area marked by yellow boxes are arrayed at the lower panel. White arrow indicated endoplasmic reticulum. **f**, Western blot analysis of the expression of IRE1α, ATF4, ATF6 and GRP78 in BMDM. **g,** Representative fluorescence images of GRP78 in BMDM and quantitative analysis of the fluorescence intensity. Scale bar, 10 μm. n = 3 biologically independent samples. **h**, Representative fluorescence images of intracellular Ca^{2+} in BMDM and quantitative analysis of Ca^{2+} levels. Scale bar, 4 μm. n = 3 biologically independent samples. **i**, Intracellular Ca^{2+} level measured by microplate reader. n = 3 biologically independent samples. **j, k**, Representative fluorescence images **(j)** and the fluorescence intensity **(k)** of LysoTracker were detected by laser scanning confocal microscopy and a microplate reader, respectively. Scale bar, 5 μm. n = 3 biologically independent samples. **l**, Representative fluorescence images of LAMP1 in BMDM and quantitative analysis of the fluorescence intensity. Scale bar, 5 μm. n = 3 biologically independent samples. **m**, Western blot analysis of the expression of proteins related to lysosomal function (ATP6V1A, ATP6V1B and LAMP1) and biogenesis (TFEB) in BMDM. **n,** The concentration of exosomes released by BMDM. n = 3 biologically independent samples. For **a, c, d, g-l,** and **n**, data are represented as the mean ± s.d. For **a, c, g-l, and n**, statistical significance was assessed by one-way ANOVA with Tukey's post-hoc test. For **d**, statistical significance was assessed by unpaired two-tailed Student's t test. *$p < 0.05$, **$p < 0.01$, ns, not significant.

We also determined whether the above mechanism functioned in *S*.a infection. Similarly, the intracellular ROS induced by *S*.a infection was observed (**Extended Data Fig.6a**), accompanied by dilated endoplasmic reticulum (**Extended Data Fig.6b**), increased expression of ERS-related proteins (**Extended Data Fig.6c, d**) and enhanced intracellular Ca^{2+} levels (**Extended Data Fig.6e, f**). These ERS effects generated by *S*.a could be abolished by 4-PBA treatment (**Extended Data Fig.6b-f**). Moreover, the ERS inhibition attenuated the elevated exosome release in macrophages induced by *S*.a infection (**Extended Data Fig.6g**). Thus, these results suggest that the mechanism by which ERS-triggered lysosomal dysfunction induced host exosome release may generally function in bacterial infection.

IRE1α-mediated lysosomal dysfunction triggers host exosome release

After determining of the fact that ERS induced by bacterial infection causes lysosome dysfunction, we then explored the specific pathway that mediates this effect. IRE1α is one of the main transmembrane ERS sensors that initiates the downstream unfolded protein response (UPR) pathway[34]. We then focused on the IRE1α pathway in lysosome function regulation based on our results, which showed upregulated IRE1α expression after infection (**Fig.5f**). To verify the role of IRE1α in this mechanism, we inhibited IRE1α expression in macrophages with IRE1α siRNA or the pharmacological inhibitor toyocamycin. We found that the expression of IRE1α and activation of the downstream Erk pathway[38] were evidently decreased in infected macrophages after treatment with IRE1α siRNA (**Fig.6a**) or toyocamycin (**Fig.6b**). Moreover, inhibition of IRE1α by siRNA or toyocamycin was accompanied by the upregulation of the levels of TFEB, LAMP1, ATP6V1A and ATP6V1B, which suggested that lysosomal function was partially recovered (**Fig.6a, b**). It has been proven that the activity of TFEB is strictly regulated through phosphorylation by Erk1/2, which inhibits the translocation of TFEB to the nucleus, where it increases the transcription of multiple genes implicated in lysosomal biogenesis, autophagy and exocytosis[37, 39, 40]. Therefore, we propose the hypothesis that macrophages develop ERS after bacterial infection, and the downstream IRE1α pathway activates Erk1/2, resulting in TFEB inactivation and declined lysosome biogenesis and function, finally promoting exosome release. To consolidate the mechanism hypothesis, lysosomal function was further investigated in infected macrophages by fluorescence imaging. The results showed reduced lysosomal acidity (**Fig.6c, d**) and decreased lysosome number (**Fig.6e**) induced by *S.*Tm infection was reversed after treatment with IRE1α siRNA or toyocamycin. More importantly, the increased exosome release caused by bacterial infection was also attenuated (**Fig.6f**). Thus, these results support the mechanism by which IRE1α in ERS induces lysosomal dysfunction, which then triggers exosome release.

We finally determined the role of ERS in lysosomal dysfunction-induced exosome release and iron metabolism *in vivo*. To enhance the pharmacological effects of the ERS inhibitor 4-PBA *in vivo*,

liposome-encapsulated 4-PBA was prepared, since liposomes are mainly taken up by macrophages in liver or spleen[41]. The drug-loading efficiency of 4-PBA in liposomes was 89.3 ± 0.13%. Fluorescence imaging showed that infused RhB-labeled liposome-encapsulated 4-PBA could be effectively transported into the liver (**Extended Data Fig.7a**) and engulfed by F4/80$^+$ macrophages *in vivo* (**Extended Data Fig.7b**) or *in vitro* (**Extended Data Fig.7c**). Subsequently, *S*.Tm-infected mice were treated with liposome-encapsulated 4-PBA to suppress ERS *in vivo* (**Fig.6g**). We found the S.Tm infection upregulated the expression of ERS-related proteins, including IRE1α, ATF6, and GRP78, in the liver (**Fig.6h**). Additionally, the fluorescence images showed that the number of F4/80$^+$/GRP78$^+$ macrophages increased significantly in the liver after infection (**Fig.6i**). The 4-PBA treatment inhibited the expression of ERS-related proteins (**Fig.6h**) and decreased the number of F4/80$^+$/GRP78$^+$ liver macrophages (**Fig.6i**). The results demonstrated that 4-PBA attenuated *S*.Tm-induced ERS in liver. More importantly, 4-PBA treatment decreased the concentration of serum exosomes (**Fig.6j**) and elevated the iron levels in infected mice (**Fig. 6k**), which indicated that ERS inhibition attenuated iron sequestration by the host. Finally, we found that 4-PBA-treated infected mice exhibited higher blood bacterial numbers (**Fig.6l**), serious liver (**Fig.6m**) and spleen injury (**Fig.6n**) accompanied by higher injury scores and a shortened lifetime (**Fig.6o**). Thus, during infection, ERS developed in host cells is required for exosome release to realize iron sequestration and infection defense.

Taken together, the findings of this study reveal how host exosomes facilitate immediate iron sequestration via a humoral regulation mechanism of iron metabolism. We found that *S*.Tm infection induces ERS and activates IRE1α signaling in macrophage, resulting in lysosomal dysfunction and immediate exosome release. These TfR-, CD163-, and CD91-bearing exosomes recycle iron to tissue-resident macrophages by binding iron-containing molecules for prompt iron sequestration. Therefore, we identify a previously unknown humoral regulation mechanism of iron metabolism during bacterial infection, reveal the role of exosomes in nutritional immunity, and suggest the release and circulation of extracellular vesicles could be an important way to promptly regulate systemic ion metabolism.

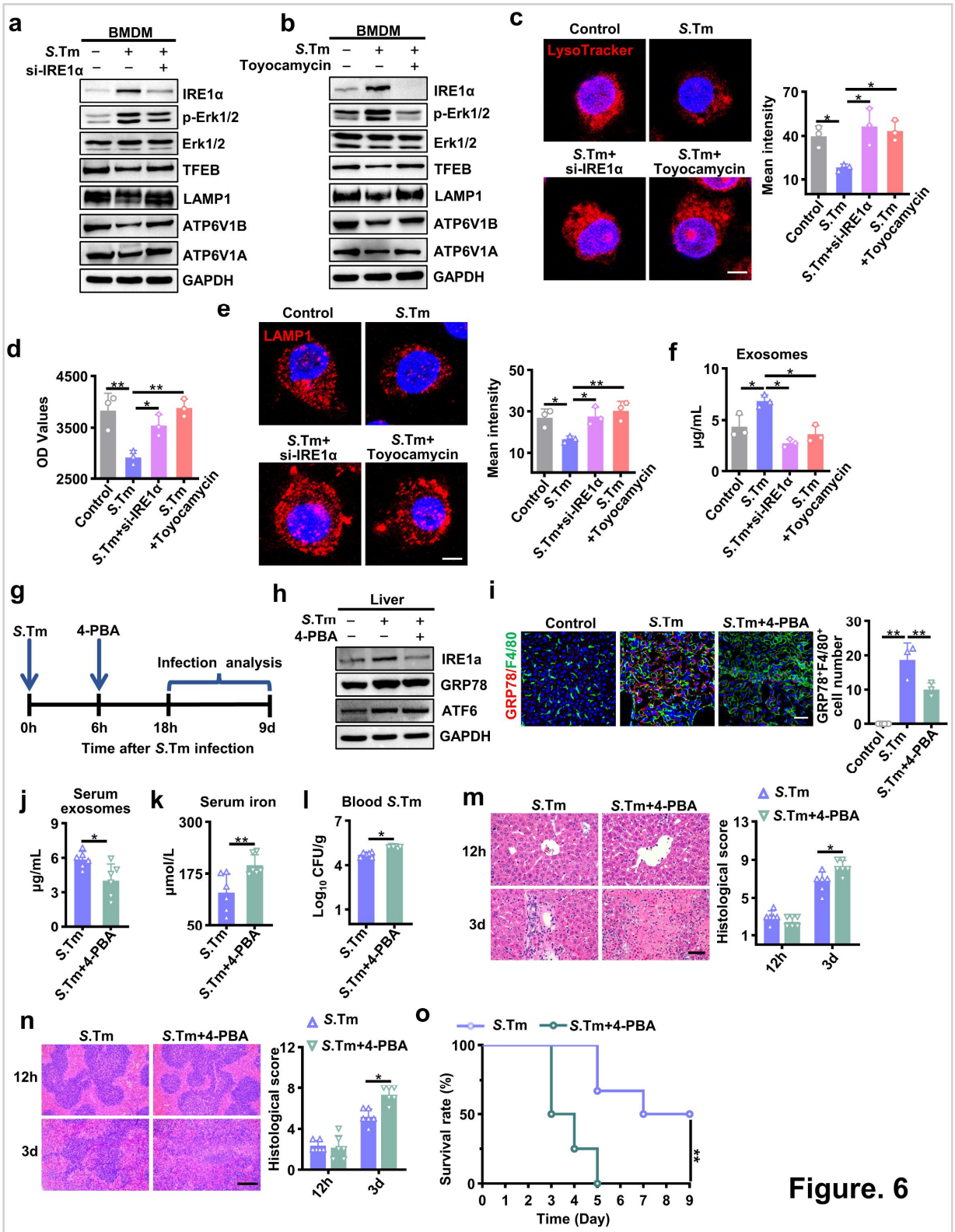

Fig. 6 IRE1α-mediated lysosomal dysfunction enhances exosome release during *S*.Tm infection.

(a-f), To inhibit the expression of IRE1α, BMDM were pretreated with IRE1α siRNA or toyocamycin and then infected with *S*.Tm for 24 hours. **a, b**, Western blot analysis of the IRE1α downstream Erk pathway and lysosomal function-related proteins in *S*.Tm-infected macrophages pretreated with IRE1α siRNA **(a)** or toyocamycin **(b)**. **c, d**, Representative fluorescence images **(c)** and the fluorescence intensity **(d)** of LysoTracker were detected by laser scanning confocal microscopy and a microplate reader, respectively. Scale bar, 5 μm. n = 3 biologically

independent samples. **e**, Representative fluorescence images of LAMP1 in BMDM and quantitative analysis of the fluorescence intensity. Scale bar, 5 μm. n = 3 biologically independent samples. **f**, The concentration of exosomes released by BMDM. n = 3 biologically independent samples. **(g-o), g,** Schematic diagram of the experimental procedure. To verify the effects of ERS on lysosomal dysfunction-induced exosome release and iron metabolism *in vivo*, empty liposomes or 4-PBA-encapsulated liposomes were injected intraperitoneally into mice 6 hours after intraperitoneal infection with *S*.Tm. After 12 hours, the mice were euthanized for further analysis. **h,** Western blot analysis of the expression of ERS-related proteins, including IRE1α, GRP78 and ATF6, in the liver. **i,** Representative fluorescence images of GRP78 level in hepatic $F4/80^+$ macrophages and quantification of the number of $F4/80^+/GRP78^+$ cells in the liver. n = 3 biologically independent samples. **j,** The concentration of exosomes in the serum. n = 6 mice. **k,** The iron level in serum. n = 6 mice. **l,** Viable count of *S*.Tm in the blood. n = 6 mice. **m, n,** Representative H&E staining of the liver **(m)** and spleen **(n)** at 12 hours and day 3 after 4-PBA injection and quantitative analysis of histological scores. scale bar, 50 μm **(m)** and 250 μm **(n)**. n = 6 mice**. o,** Survival rates of mice. n = 6 mice. For **c-f** and **i-n**, data are represented as the mean ± s.d. For **c-f** and **i**, statistical significance was assessed by one-way ANOVA with Tukey's post-hoc test. For **j** and **l-n**, statistical significance was assessed by unpaired two-tailed Student's t test. For **k**, statistical significance was assessed by the Mann–Whitney U test. For **o**, statistical significance was assessed by the log-rank test. $^*p < 0.05$, $^{**}p < 0.01$, ns, not significant.

Discussion

Iron is needed to fulfill multiple biological functions in living organisms due to its unique chemical properties[42]. Iron in host cells also acts as a signal to induce the generation of hydroxyl radicals and therefore kill intracellular pathogens[43,44]. Unsurprisingly, given its remarkable versatility and critical functions in biological systems, fierce competition for iron between the host and pathogen takes place under infection conditions. Successful invaders launched highly efficient machinery, including siderophore and hemophore systems, to capture iron from host iron sources[45]. To effectively inhibit the growth of bacterial pathogens, the host simultaneously evolves sophisticated defense mechanisms that restrict iron availability for bacterial pathogens and thereby limit their infection. The host employs siderophilins, including transferrin and lactoferrin, to transport iron to storage sites to limit iron uptake by the bacteria[46]. Moreover, host cells can release lipocalin-2 to obstruct the iron-acquiring strategy of bacteria[47]. While given that iron-containing proteins existing in body fluid can be acquired by the bacteria[2], it is important to explore how the host promptly acquire and preserve iron for rapid iron sequestration after infection.

For every tactic employed by invading pathogens to acquire iron, the host evolves relevant defense

mechanisms. Interestingly, recent studies show that bacterial pathogens can release extracellular vesicles such as outer membrane vesicles (OMVs) to acquire iron from their hosts. OMVs carry degradative enzymes and specific receptors that enable bacteria to efficiently acquire iron and thus to facilitate bacterial survival[48]. Therefore, it is worth wondering if the intelligent host also developed a similar strategy to enhance the efficiency of iron sequestration by arranging decoys in the circulation. It has been proven that the total number of exosomes is significantly increased during bacterial infection[13,49]. While most of the studies on exosomes in bacterial infection have focused on the mechanisms for antigen presentation or signal transduction[50], other biological functions of exosomes still need to be explored. A recent study provided evidence to support that exosomes confer a benefit or survival advantage to their parental cells by serving as decoys to trap and neutralize bacterial toxins[13]. This study suggests that exosomes can exert their biological functions by specific membrane receptor binding capacity. Here, we found that host cells immediately release exosomes to bind iron after infection, prevent the bacteria from iron acquisition, and deliver iron to tissue-resident macrophages for prompt iron sequestration. The findings of our study reveal a previously unknown humoral regulation mechanism of iron metabolism during bacterial infection, broaden the knowledge of iron metabolism as cellular and humoral manner. Moreover, the findings show that host cell send circulating “weapons” to compete with bacteria for iron, suggesting the evolutionary conservative functions of extracellular vesicles for iron acquisition in both prokaryotes and eukaryotes.

Exosome release in host cells is ubiquitous and critical for an assortment of physiological and pathological processes[51]. Exosomes contain a broad array of biomolecules, including proteins, lipids and nucleic acids[51]. These nanosized exosomes are able to diffuse long distances in a given time and fuse with targeted cells[12]. The combination of these features allows exosomes to serve as natural delivery vehicles[52]. One of the key features of exosomes is that they have a large surface compared to volume[53]. Therefore, surface properties or molecular interactions at the surface of exosomes may perform important functions. In this study, we found that TfR, CD163, and CD91 are integrated on the exosome surface, which ensure the iron recycling capacity of exosomes through capture of the iron-containing molecules to facilitate iron recycling. These “iron catchers” enhance the efficiency in iron sequestration and resistance to bacterial infection, thereby

highlighting a previously unknown mechanism of innate immunity. The results of this study suggest that infusing TfR-, CD163-, and CD91-bearing exosomes provides a potential strategy for combating with bacterial infection. Although herein we focus on exosomes, it is also important to evaluate the role of other kinds of extracellular vesicles, including microvesicles or apoptotic bodies, in iron metabolism and infection defense since bacterial infection may also regulate other kinds of extracellular vesicles release[50]. In this study, we mainly focused on the exosomes derived from macrophages. In fact, circulating exosomes from other origins may also participate in iron metabolism regulation via membrane receptors. Meanwhile, whether exosomes in the circulation regulate other kinds of nutrients or small molecules still needs to be determined, future studies may provide more evidence for extracellular vesicle-based metabolism regulation.

Methods

Bacterial Strains and Growth Conditions

Salmonella typhimurium strain (*S*.Tm, ATCC14028) and staphylococcus aureus (*S*.a, ATCC6538) were purchased from Beijing Beina Biological Co., Ltd. *S*.Tm and *S.a* were grown overnight in Luria-Bertani (LB) broth (10 g tryptone, 5 g yeast extract, 10 g NaCl per liter) at 37℃ with shaking. Bacteria density was confirmed by dilution plating. To obtain heat-killed *S*.Tm (HK*S*.Tm), *S*.Tm were cultured in LB broth for overnight at 37℃, and centrifuged in 4000×g for 5min and resuspended in PBS. The resuspended bacteria were boiled at 70℃ for 1 h before being used immediately.

Cell culture

Bone marrow-derived macrophages (BMDM) were obtained by harvesting bone marrow from femurs and tibias of C57BL/6J wide-type mice. Bone marrow cells were flushed out with PBS and lysed with red blood cell lysing buffer (Beyotime). After centrifuging for 5 min at 800×g, the cells were seeded in plates and incubated with Dulbecco's modified Eagle medium (DMEM) containing 10% fetal bovine serum (FBS) and 20 ng/ml macrophage colony-stimulating factor (M-CSF) (PeproTech). Mature BMDM were used for the next experiments until 7-8 days. Mature BMDM were infected with *S*.Tm at the multiplicity of infection [MOI (bacteria per macrophage)] of 10. Cells were incubated in DMEM without FBS and antibiotic. After incubating for 30 min, the cells

were washed with PBS and replaced with fresh DMEM containing 10% exosome-depleted FBS. Mock-infected wells received an equivalent volume of PBS. For *S.*a infection, BMDM were infected with *S.*a at MOI of 25 for 1h. Subsequently, extracellular bacteria were removed by washing with PBS. BMDM were cultured in fresh DMEM containing 10% exosome-depleted FBS. When indicated, 5 mmol/L 4-Phenylbutyric acid (4-PBA) (MedChemExpress) was applied to pretreat the BMDM for 2 h before *S.*Tm infection. For experiments using bafilomycin A1 (MedChemExpress), mature BMDM were pretreated with 100 nM bafilomycin A1 as the positive control of lysosomal dysfunction.

siRNA and transfection

BMDM were transfected with siRNA (RiBOBIO) targeting TfR and IRE1α mRNAs using the Advanced DNA RNA Transfection Reagent (Zeta life) according to the manufacturer's instruction. Subsequent treatments on transfected cells were performed 24 h post-transfection.

Preparation and characterization of liposome-encapsulated 4-PBA

According to the procedure previously describe by Chen et al[54], liposomes-encapsulated 4-PBA was prepared with hydrogenated soybean phosphotidylcholine (Sinopharm) and cholesterol (Sinopharm) by ethanol injection method. Subsequently, to estimate encapsulation efficiency for liposome-encapsulated 4-PBA, 4-PBA was labeled by RhB, the content of 4-PBA was analyzed by the fluorescence spectrometry (PerkinElmer, USA).

Animal experiment

All animal experiments were approved by the Animal Care Committee of the Fourth Military Medical University, China. Wide-type 6-8 week-old female C57BL/6J were obtained from the Laboratory Animal Research Center of the Fourth Military Medical University, Xi'an, China. To identify the function of exosomes in *S.*Tm infection, mice were pre-injected intraperitoneally (*i.p.*) with GW4869 (MedChemExpress) at dose of 1.5 μg/g for 6h, followed by an i.p. injection of 3×10^5CFU of *S.*Tm. To analyze early changes in serum iron, mice were euthanized at 12h after infection. Mice received injections of PBS as control. The survival rate of the mice was monitored every 12 h for a s period of 9 day. To further verify the effects of exosome release on *S.*Tm infection,

the above mice that received GW4869 and *S*.Tm were then intravenously injected with exosomes (100 μg) 1h and 6h after the *S*.Tm infection. These exosomes used for the experiments were isolated from the supernatant of uninfected or infected BMDM or from the serum of uninfected or infected mice. Mice were euthanized at 24 h after infection. The survival rate of the mice was monitored every 12 h for 7 days.

To test the effect of endogenous exosomes on the metabolism of iron, mice were intraperitoneally infected with 3 $\times 10^7$CFU heat-killed S. typhimurium (HK*S*.Tm) to induce endogenous exosome release. After 3h, these mice were injected with GW4869 at dose of 4μg/g body weight. After 3h, above mice were then injected with 3×10^5CFU of *S*.Tm. Mice were then euthanized at 12 h for exploring the levels of serum iron and exosomes, and the number of bacteria. The survival rate of mice was recorded for 9 days post-infection. In addition, to verify the effect of serum iron on the infection, mice were pre-treated with HK*S*.Tm 3 h prior to an injection of iron-dextran (125 μg/g body weight, Sigma). After 3h, these mice were subsequently infected with *S*.Tm. Mice were euthanized at 12 h for exploring the changes of bacteria in blood. The survival rate of mice was monitored for 8 days. To verify the effect of endoplasmic reticulum stress on exosome release, mice were treated with 3×10^5CFU of *S*.Tm. At 6h after infection, mice were injected with (10 mg/kg body weight) liposome-encapsulated 4-PBA or equivalent volume of empty liposome. To test the changes in iron and exosomes, blood and tissues were collected at 12h after 4-PBA injection.

The determination of bacteria burden in blood

The blood was collected in the tube with heparin sodium to prevent blood from coagulation. Bacteria CFU were counted by plating dilutions of blood on LB plates containing 1.5% agar and enumerating the bacteria colonies after incubation at 37℃.

Serum and tissue iron measurements

Blood was collected into EP tubes and allowed to clot at 4℃ for 12 h followed by centrifugation at 2500 rpm for 10 mins. The serum was used for iron level analysis. For liver and spleen iron measurements, the tissue was mixed with iron assay buffer. After homogenization, the mixture was centrifuged at 16000×g for 10 min at 4℃, and the supernatant was used for iron assay. The total

iron was detected using an Iron Assay Kit according to the manufacturer's instructions (Abcam). In brief, 1-50 µl serum or other liquid samples were added to the 96-well plate and brought the volume to 100 µl per well with Assay Buffer. Iron reducer was then added to each of the sample wells and incubated in dark for 30 min at 37°C. After first incubation, 100 µl of iron probe was added to each well and incubated in dark for 60 min at 37°C. Absorbance was measured at 593 nm using microplate reader (Bio-Rad, USA).

Histopathological evaluation

The liver and spleen samples were placed in 4% paraformaldehyde (PFA) overnight at 4°C, imbedded in paraffin blocks, sliced to 4-µm thick section, and stained with hematoxylin and eosin (HE). After staining, the sections were evaluated with Leica DM4B Microscope (Leica). The liver injury degree was determined by the histological scoring analysis. The assessment was expressed as the sum of the individual score grades of 0 (normal), 1 (mild injury), 2 (moderate injury), 3 (severe injury) and 4 (maximum injury) for each of the following five categories: inflammation infiltration, cytoplasm vacuolization, nuclear condensation, hemorrhage, and hepatocyte necrosis. To evaluate the splenic histological changes, a semi-quantitative scoring system was used. The histopathological changes in spleen were classified based on the severity of three histological criteria: architecture loss, necrotic cells, and inflammation. The histopathological changes were graded on a scale as follows: absent (0), slight (1), moderate (2), and pronounced (3).

Immunofluorescence staining

For tissues, liver or spleen was fixed in 4% PFA for 24 h. After washing with PBS, the samples were immersed in 30% sucrose solution for 24 h, and then embedded in optimum cutting temperature (OCT) compound (Tissue OCT-Freeze Medium). The tissues were prepared as 10-µm sections. After permeation with 0.1% Triton X-100 (Sigma), cryosections were blocked with goat serum (Boster) for 1 h at room temperature. Then, cryosections were incubated with the following antibodies: anti-F4/80 antibody (1:200, ab6640, Abcam), Anti-GRP78/Bip antibody (1:200, ab21658, Abcam), and anti-Macrophage antibody (1:200, ab22506, Abcam) at 4°C overnight. After washing with PBS, the sections were incubated with Alexa Fluor 488/594-conjugated secondary antibodies (1:200, YeaSen) at 37°C for 1 h, followed by staining with Hoechst 33342 for 10 min.

Finally, the immunofluorescence images were obtained by confocal laser scanning microscopy (CLSM) (Nikon).

For cells, BMDM were grown in 24-well plates containing coverslips before indicated treatments. After treatment, the cells were washed with PBS, fixed with 4% PFA for 30 min, and blocked with 5%BSA for 1h at room temperature. The cells were then incubated with anti-F4/80 antibody (1:200), or anti-GRP78/Bip antibody (1:200), or anti-LAMP1 antibody (1:200, ab24170, Abcam) overnight at 4℃ followed by incubation with secondary antibody. The cells were stained with Hoechst and visualized by CLSM. To analyze the ROS levels in cells, Reactive Oxygen Species Assay Kit (50101ES01, YeaSen) was used. Cells were harvested at the indicated time points and washed with PBS. Then, cells were incubated with DCFH-DA at a final concentration of 10 μM at 37℃ for 30 min in the dark. After washing with PBS, cells were fixed with 4% PFA for 30 min at 4 °C. Finally, cells were stained with Hoechst and visualized by CLSM.

Intracellular Ca^{2+} measurement

To analyze the intracellular Ca^{2+} levels in cells, BMDM were loaded with the cell permeant Ca^{2+} indicator Fluo-4, AM (40704ES50, YeaSen) in calcium-free Hank's balanced salt solution (HBSS) at a final concentration of 5 μM for 30 min (37℃). The green fluorescence of Ca^{2+} was measured with a multimode plate reader (PerkinElmer, USA) and CLSM (Nikon, Japan).

LysoTracker fluorescence measurement

To measure the lysosomal acidity, cells were incubated in serum-free medium with 50 nM lysoTracker (40739ES50, YeaSen) at 37℃ for 30 min. After washing with PBS, lysotracker fluorescence intensity was measured with a multimode plate reader (PerkinElmer, USA) and CLSM (Nikon, Japan).

Exosome isolation and characterization

Cell supernatant or serum was centrifuged at 800×g for 5 min to remove cells or cell debris. The supernatant was then centrifuged at 16000×g for 30 min to remove microvesicles. Then, the supernatant was ultracentrifuged at 4℃ for 70 min at a speed of 150000×g, and followed by washing with PBS and purification by ultracentrifugation at 150000×g for 70 min. Exosomes were

gathered from the bottom of the tube. The protein concertation was measured by BCA kit (Beyotime). The size of exosomes was examined using nanoparticle tracking analysis (NTA) with Zeta View PMX 110 (Particle Metrix) and corresponding software Zeta View 8.04.02.

Electron microscopy

For transmission electron microscopy, a drop of suspension containing exosomes was applied to a 200-mesh carbon-stabilized copper grids. Exosomes were allowed to absorb for 5 min before the excess suspension was wicked off. Next, the grid was stained with 2% phosphotungstic acid hydrate for 30 s followed by washing with distilled water for three times. Excess solution was wicked off, and the grid was allowed to air-dry before observation. For immunogold staining, exosomes were mixed with an equal volume of 2.54% glutaraldehyde for 20 min at room temperature, and then applied to 200 mesh nickel grids. After blocking with 5% BSA, the grid was incubated with a 1:20 dilution of the primary antibody (anti-CD163 antibody, anti-CD91 antibody, anti-TfR antibody) for 1h at room temperature. After washing with ultra-pure water, the grid was treated with 10-nm gold-labeled secondary antibody (Electron Microscopy Sciences) for 30 min. The grid was then washing with ultra-pure water, and stained with 2% phosphotungstic acid hydrate for 30 s, followed by rinsing with ultra-pure water. After dying, all grids were examined with TEM (TECNAI Spirit, FEI).

***In vitro* and *in vivo* fluorescence tracing of exosomes and liposome-encapsulated 4-PBA**

For *in vitro* tracing of liposome-encapsulated 4-PBA in macrophage, BMDM were treated with Rhodamine B-labeled (RhB) liposome-encapsulated 4-PBA for 3 h. The cells were then washed with PBS and fixed with 4%PFA for 30 min at room temperature. The cells were blocked with 5%BSA, incubated with F4/80 antibody at 4℃ overnight, and treated with Alexa Fluor 488-conjugated secondary antibodies. The cell nuclei were counter-stained with Hoechst 33342. At the end of the experiment, the cells were washed with PBS and observed using the CLSM. For *ex vivo* fluorescence tracing of exosomes and liposome-encapsulated 4-PBA, DiR-labeled exosomes or RhB-labeled liposome-encapsulated 4-PBA were administrated into mice via intravenous or intraperitoneal injection, respectively. After 24 h, mice were euthanized and organs were collected and subjected to *ex vivo* bioluminescence imaging performed by an In Vivo Imaging System

(Xenogen). The luminescent signal was evaluated manually using Living Image Software (Caliper LifeSciences). To verify the specific uptake of exosomes by *S*.Tm, *S*.Tm expressing mCherry (*S*. Typhimurium-mCherry) were treated with PKH-67-labeled exosomes for 3 h. Then, the bacterial suspension containing exosomes was smeared thinly on a glass slide and observed by the CLSM.

Iron-binding assay

Normal mouse serum was collected, and the serum exosomes were removed by ultracentrifugation at 150000×g for 70min at 4℃. The exosome-depleted serum was added with exosomes from the supernatant of uninfected, infected BMDM or serum. After incubation overnight at 4℃, the added exosomes were isolated by ultracentrifugation at 150000×g for 70 min at 4℃. The serum supernatant and the exosomal fraction were respectively collected. The total iron levels in supernatant were measured by Iron Assay Kit (Abcam). And the transferrin levels in supernatant were analyzed by ELISA (Elabscience). In addition, the serum supernatant was heated at 56℃ for 1h and *S*. Tm or *S*.a were inoculated into the supernatant. The cultures were then maintained under continuous shaking at 37℃ with optical measurements at OD_{490} or OD_{620} every 12 hours.

Quantification of transferrin in serum and exosomes

To expose the transferrin protein in the exosomal fraction, the exosomal fraction was suspended 1% Triton X-100 for 30 min at room temperature. After centrifuging at 12000×g for 10 min, the exosome lysates were collected. The levels of transferrin were measured in serum and the exosomal lysates using ELISA kit (Elabscience) according to the manufacturer's instruction.

Western blot

The samples were lysed on ice in lysis buffer (Beyotime) containing a protease inhibitor for 30 min. Proteins samples (20 μg) quantified by BCA assay were loaded on the 8%-12% of SDS-polyacrylamide gel, and then transferred to PVDF membrane (Merck Millipore) for 2 h. The membrane was blocked with 5% BSA at room temperature for 1 h, and then incubated with primary antibody overnight at 4℃. The membranes were then incubated with HRP-labeled secondary antibody for 1 h at room temperature and was processed by chemiluminescent kit (Merck Millipore) with an image system (Tanon 4600). The anti-CD81 antibody (ab109201), anti-TSG101 antibody

(ab125011), anti-Calnexin antibody (ab22595), anti-Transferrin Receptor antibody(ab84036), anti-CD91 antibody(ab92544), anti-CD163 antibody (ab182422), anti-ATF6 antibody (ab203119), anti-ATP6V1A antibody (ab199326), anti-GRP78 antibody(ab21658), anti-LAMP1 antibody(ab24170), and anti-ATP6V1B antibody (ab200839) were purchased from Abcam. The anti-CD63 antibody (sc-5275) were obtained from Santa Cruz. The anti-Alix antibody (#92880), anti-ATF4 antibody (#11815), anti-IRE1α antibody (#3294P), anti-TFEB antibody (#4240), anti-Erk1/2 antibody (#9102s), and anti-Phospho-Erk1/2 antibody (#9101s) were purchased from Cell Signaling Technology. The anti-GAPDH antibody was obtained from YeaSen. The secondary antibodies [peroxidase AffiniPure goat anti-mouse immunoglobulin G (IgG), DY60203; peroxidase AffiniPure goat anti-rabbit IgG, DY60202] were all purchased from DIYIBio.

Data presentation and statistical analysis

Data was presented as the mean ± s.d, and analyzed using the SPSS 19.0 software. For all tests, differences of $p<0.05$ were considered significant. Unpaired two-tailed Student's t test and Mann-whitney U-test were used for comparing two groups. One-way ANOVA with Tukey's correction or Kruskal-Wallis test was used for comparisons among multiple groups, wherever applicable. Survival functions were compared using the log-rank test.

References

1. Thornton, F.J., Schäffer, M.R. & Barbul, A. Wound healing in sepsis and trauma. *Shock* **8**, 391-401 (1997).

2. Cassat, J.E. & Skaar, E.P. Iron in infection and immunity. *Cell Host Microbe* **13**, 509-519 (2013).

3. Wang, J. & Pantopoulos, K. Regulation of cellular iron metabolism. *Biochem J* **434**, 365-381 (2011).

4. Soares, M.P. & Hamza, I. Macrophages and Iron Metabolism. *Immunity* **44**, 492-504 (2016).

5. Kalluri, R. The biology and function of exosomes in cancer. *J Clin Invest* **126**, 1208-1215 (2016).

6. Brahmer, A. Neuberger, E., Esch-Heisser, L., Haller, N., Jorgensen, M. M., Baek, R, Möbius, W., Simon, P., & Krämer-Albers, E.M. Platelets, endothelial cells and leukocytes contribute to the exercise-triggered release of extracellular vesicles into the circulation. *J Extracell Vesicles* **8**, 1615820 (2019).

7. Bhatnagar, S. & Schorey, J.S. Exosomes released from infected macrophages contain Mycobacterium avium glycopeptidolipids and are proinflammatory. *Journal of Biological Chemistry* **282**, 25779-25789 (2007).

8. Bhatnagar, S., Shinagawa, K., Castellino, F.J. & Schorey, J.S. Exosomes released from macrophages infected with intracellular pathogens stimulate a proinflammatory response in vitro and in vivo. *Blood, The Journal of the American Society of Hematology* **110**, 3234-3244 (2007).

9. Verweij, F.J. Revenu, C., Arras, G., Dingli, F., Loew, D., Pegtel, D. M., Follain, G., Allio, G., Goetz, J. G., Zimmermann, P., Herbomel, P., Del Bene, F., Raposo, G., & van Niel,. Live Tracking of Inter-organ Communication

by Endogenous Exosomes In Vivo. *Dev Cell* **48**, 573-589.e574 (2019).

10. Villarroya-Beltri, C. *et al.* ISGylation controls exosome secretion by promoting lysosomal degradation of MVB proteins. *Nature Communications* **7**, 13588 (2016).

11. Jeppesen, D.K. Fenix, A. M., Franklin, J. L., Higginbotham, J. N., Zhang, Q., Zimmerman, L. J., Liebler, D. C., Ping, J., Liu, Q., Evans, R., Fissell, W. H., Patton, J. G., Rome, L. H., Burnette, D. T., & Coffey, R. J. Reassessment of Exosome Composition. *Cell* **177**, 428-445.e418 (2019).

12. Kastelowitz, N. & Yin, H. Exosomes and microvesicles: identification and targeting by particle size and lipid chemical probes. *Chembiochem* **15**, 923-928 (2014).

13. Keller, M.D. Ching, K. L., Liang, F. X., Dhabaria, A., Tam, K., Ueberheide, B. M., Unutmaz, D., Torres, V. J., & Cadwell, K.. Decoy exosomes provide protection against bacterial toxins. *Nature* **579**, 260-264 (2020).

14. Drakesmith, H. & Prentice, A.M. Hepcidin and the iron-infection axis. *Science* **338**, 768-772 (2012).

15. Shutinoski, B. Hakimi, M., Harmsen, I. E., Lunn, M., Rocha, J., Lengacher, N., Zhou, Y. Y., Khan, J., Nguyen, A., Hake-Volling, Q., El-Kodsi, D., Li, J., Alikashani, A., &Schlossmacher, M. G. Lrrk2 alleles modulate inflammation during microbial infection of mice in a sex-dependent manner. *Sci Transl Med* **11,** eaas9292 (2019).

16. Wang, L. Harrington, L., Trebicka, E., Shi, H. N., Kagan, J. C., Hong, C. C., Lin, H. Y., Babitt, J. L., & Cherayil, B. J.. Selective modulation of TLR4-activated inflammatory responses by altered iron homeostasis in mice. *J Clin Invest* **119**, 3322-3328 (2009).

17. Kim, D.K. Jeong, J. H., Lee, J. M., Kim, K. S., Park, S. H., Kim, Y. D., Koh, M., Shin, M., Jung, Y. S., Kim, H. S., Lee, T. H., & Choi, H. S.. Inverse agonist of estrogen-related receptor γ controls Salmonella typhimurium infection by modulating host iron homeostasis. *Nat Med* **20**, 419-424 (2014).

18. Essandoh, K. Yang, L., Wang, X., Huang, W., Qin, D., Hao, J., Wang, Y., Zingarelli, B., Peng, T., & Fan, G. C.. Blockade of exosome generation with GW4869 dampens the sepsis-induced inflammation and cardiac dysfunction. *Biochim Biophys Acta* **1852**, 2362-2371 (2015).

19. Iguchi, Y. Eid, L., Parent, M., Soucy, G., Bareil, C., Riku, Y., Kawai, K., Takagi, S., Yoshida, M., Katsuno, M., Sobue, G., & Julien, J. P. Exosome secretion is a key pathway for clearance of pathological TDP-43. *Brain* **139**, 3187-3201 (2016).

20. Walker, J. Dichter, E., Lacorte, G., Kerner, D., Spur, B., Rodriguez, A., & Yin, K.. Lipoxin a4 increases survival by decreasing systemic inflammation and bacterial load in sepsis. *Shock* **36**, 410-416 (2011).

21. Gan, Z. Tang, X., Wang, Z., Li, J., Wang, Z., & Du, H.. Regulation of macrophage iron homeostasis is associated with the localization of bacteria. *Metallomics* **11**, 454-461 (2019).

22. Kapetanovic, R. Fairbairn, L., Beraldi, D., Sester, D. P., Archibald, A. L., Tuggle, C. K., & Hume, D. A.. Pig bone marrow-derived macrophages resemble human macrophages in their response to bacterial lipopolysaccharide. *J Immunol* **188**, 3382-3394 (2012).

23. Winn, N.C., Volk, K.M. & Hasty, A.H. Regulation of tissue iron homeostasis: the macrophage "ferrostat". *JCI Insight* **5** (2020).

24. Mayhew, T.M. & Lucocq, J.M. Developments in cell biology for quantitative immunoelectron microscopy based on thin sections: a review. *Histochem Cell Biol* **130**, 299-313 (2008).

25. Ratledge, C. & Dover, L.G. Iron metabolism in pathogenic bacteria. *Annu Rev Microbiol* **54**, 881-941 (2000).

26. Nairz, M., Schroll, A., Sonnweber, T. & Weiss, G. The struggle for iron - a metal at the host-pathogen interface. *Cell Microbiol* **12**, 1691-1702 (2010).

27. Otto, B.R., Verweij-van Vught, A.M. & MacLaren, D.M. Transferrins and heme-compounds as iron sources for pathogenic bacteria. *Crit Rev Microbiol* **18**, 217-233 (1992).

28. Dichtl, S. Demetz, E., Haschka, D., Tymoszuk, P., Petzer, V., Nairz, M., Seifert, M., Hoffmann, A., Brigo, N., Würzner, R., Theurl, I., Karlinsey, J. E., Fang, F. C., & Weiss, G. Dopamine Is a Siderophore-Like Iron Chelator That Promotes Salmonella enterica Serovar Typhimurium Virulence in Mice. *mBio* **10** (2019).

29. Haley, K.P. & Skaar, E.P. A battle for iron: host sequestration and Staphylococcus aureus acquisition. *Microbes Infect* **14**, 217-227 (2012).

30. Lokken, K.L., Tsolis, R.M. & Bäumler, A.J. Hypoferremia of infection: a double-edged sword? *Nat Med* **20**, 335-337 (2014).

31. Arezes, J. Jung, G., Gabayan, V., Valore, E., Ruchala, P., Gulig, P. A., Ganz, T., Nemeth, E., & Bulut, Y. Hepcidin-induced hypoferremia is a critical host defense mechanism against the siderophilic bacterium Vibrio vulnificus. *Cell Host Microbe* **17**, 47-57 (2015).

32.Ganz, T. Iron in innate immunity: starve the invaders. *Curr Opin Immunol* **21**, 63-67 (2009).

33. Liao, Z. Liu, Z., Gong, Z., Hu, X., Chen, Y., Cao, K., Zhang, H., Gan, L., Chen, J., Yang, Y., & Cai, J. Heat-killed Salmonella Typhimurium protects mice against carbon ion radiation. *J Int Med Res* **48**, 300060520924256 (2020).

34. Rashid, H.O., Yadav, R.K., Kim, H.R. & Chae, H.J. ER stress: Autophagy induction, inhibition and selection. *Autophagy* **11**, 1956-1977 (2015).

35. Moretti, J. Roy, S., Bozec, D., Martinez, J., Chapman, J. R., Ueberheide, B., Lamming, D. W., Chen, Z. J., Horng, T., Yeretssian, G., Green, D. R., & Blander, J. M. STING Senses Microbial Viability to Orchestrate Stress-Mediated Autophagy of the Endoplasmic Reticulum. *Cell* **171**, 809-823 e813 (2017).

36. Zhang, Y. Cen, J., Jia, Z., Hsiao, C. D., Xia, Q., Wang, X., Chen, X., Wang, R., Jiang, Z., Zhang, L., & Liu, K.. Hepatotoxicity Induced by Isoniazid-Lipopolysaccharide through Endoplasmic Reticulum Stress, Autophagy, and Apoptosis Pathways in Zebrafish. *Antimicrob Agents Chemother* **63** (2019).

37. Settembre, C. Di Malta, C., Polito, V. A., Garcia Arencibia, M., Vetrini, F., Erdin, S., Erdin, S. U., Huynh, T., Medina, D., Colella, P., Sardiello, M., Rubinsztein, D. C., & Ballabio, A.. TFEB links autophagy to lysosomal biogenesis. *Science* **332**, 1429-1433 (2011).

38. Nguyên, D.T. Kebache, S., Fazel, A., Wong, H. N., Jenna, S., Emadali, A., Lee, E. H., Bergeron, J. J., Kaufman, R. J., Larose, L., & Chevet, E.. Nck-dependent activation of extracellular signal-regulated kinase-1 and regulation of cell survival during endoplasmic reticulum stress. *Mol Biol Cell* **15**, 4248-4260 (2004).

39. Martina, J.A., Chen, Y., Gucek, M. & Puertollano, R. MTORC1 functions as a transcriptional regulator of autophagy by preventing nuclear transport of TFEB. *Autophagy* **8**, 903-914 (2012).

40. Roczniak-Ferguson, A. Petit, C. S., Froehlich, F., Qian, S., Ky, J., Angarola, B., Walther, T. C., & Ferguson, S. M.. The transcription factor TFEB links mTORC1 signaling to transcriptional control of lysosome homeostasis. *Sci Signal* **5**, ra42 (2012).

41. Hua, S. & Wu, S.Y. The use of lipid-based nanocarriers for targeted pain therapies. *Front Pharmacol* **4**, 14(2013).

42. Caza, M. & Kronstad, J.W. Shared and distinct mechanisms of iron acquisition by bacterial and fungal pathogens of humans. *Front Cell Infect Microbiol* **3**, 80 (2013).

43. Patruta, S.I. & Hörl, W.H. Iron and infection. *Kidney Int Suppl* **69**, S125-130 (1999).

44. Sarwar, H. S., Akhtar, S., Sohail, M. F., Naveed, Z., Rafay, M., Nadhman, A., Yasinzai, M., & Shahnaz, G. (2017). Redox biology of Leishmania and macrophage targeted nanoparticles for therapy. *Nanomedicine (London, England)*, **12**(14), 1713–1725..

45. Wandersman, C. & Delepelaire, P. Bacterial iron sources: from siderophores to hemophores. Annu Rev Microbiol 58, 611-647 (2004).

46. Hood, M.I. & Skaar, E.P. Nutritional immunity: transition metals at the pathogen-host interface. *Nat Rev Microbiol* **10**, 525-537 (2012).

47. Xiao, X., Yeoh, B.S. & Vijay-Kumar, M. Lipocalin 2: An Emerging Player in Iron Homeostasis and Inflammation. *Annu Rev Nutr* **37**, 103-130 (2017).

48. Lin, J., Zhang, W., Cheng, J., Yang, X., Zhu, K., Wang, Y., Wei, G., Qian, P. Y., Luo, Z. Q., & Shen, X.. A Pseudomonas T6SS effector recruits PQS-containing outer membrane vesicles for iron acquisition. *Nat Commun* **8**, 14888 (2017).

49. Carrière, J., Bretin, A., Darfeuille-Michaud, A., Barnich, N. & Nguyen, H.T.T. Exosomes released from cells infected with crohn's disease–associated adherent-invasive Escherichia Coli activate host innate immune responses and enhance bacterial intracellular replication. *Inflammatory Bowel Diseases* **22**, 516-528 (2016).

50. Schorey, J.S., Cheng, Y., Singh, P.P. & Smith, V.L. Exosomes and other extracellular vesicles in host-pathogen interactions. *EMBO Rep* **16**, 24-43 (2015).

51. Kalluri, R. & LeBleu, V.S. The biology, function, and biomedical applications of exosomes. *Science* **367**(2020).

52. Wortzel, I., Dror, S., Kenific, C.M. & Lyden, D. Exosome-mediated metastasis: Communication from a distance. *Dev Cell* **49**, 347-360 (2019).

53. Buzás, E.I., Tóth, E., Sódar, B.W. & Szabó-Taylor, K. Molecular interactions at the surface of extracellular vesicles. *Semin Immunopathol* **40**, 453-464 (2018).

54. Chen, Y.Q., Zhu, W. T., Lin, C. Y., Yuan, Z. W., Li, Z. H., Yan, P. K. Delivery of rapamycin by liposomes synergistically enhances the chemotherapy effect of 5-fluorouracil on colorectal cancer. *Int J Nanomedicine* **16**, 269-281 (2021).

Acknowledgements

This work was supported by the National Natural Science Foundation of China (no.82170925 to Sh.L., no.81991504 to Y.J. and no.31800817 to Si.L.), and National Key Research and Development Program of China (no. 2016YFC1101400 to Y.J.).

Author contributions

H.K. and G.D. designed, performed and interpreted the experiments and wrote the manuscript. L.C. and X.W. performed bacterial experiments and characterized properties of liposome. H.X., X.L., F.D. assisted with animal experiments. X.Y. and Si.L. performed the histopathological studies and collected data. L.B., H.L., and B.L. contributed to data analysis and interpretation. Sh.L. developed the original concept. Sh.L. and Y.J. conceived the study and supervised the experiments.

Competing interests

The authors declare no competing interests.

Supplementary Files

This is a list of supplementary files associated with this preprint. Click to download.

- SupplementaryInformation.pdf